X-525-66-262

NASA TM X-55580

A TWO-CHANNEL MONOPULSE REFLECTOR ANTENNA SYSTEM WITH A MULTIMODE LOGARITHMIC SPIRAL FEED

JUNE 1966

NASA — GODDARD SPACE FLIGHT CENTER —

GREENBELT, MD.

X-525-66-262

A TWO-CHANNEL MONOPULSE REFLECTOR ANTENNA SYSTEM WITH A MULTIMODE LOGARITHMIC SPIRAL FEED

Paul A. Lantz
Advanced Development Division

June 1966

GODDARD SPACE FLIGHT CENTER
Greenbelt, Maryland

A TWO-CHANNEL MONOPULSE REFLECTOR ANTENNA SYSTEM WITH A MULTIMODE LOGARITHMIC SPIRAL FEED

Paul A. Lantz
Advanced Development Division

ABSTRACT

It is possible to excite multiarm planar logarithmic spiral antennas in various modes. These antennas can be used to feed reflectors for monopulse tracking and space data acquisition. This report reviews the basic theory of operation of these antennas, expands it, and describes a two-channel monopulse antenna system using a feed of this type. It also describes performance of an operational 85-foot diameter reflector antenna and discusses limitations of performance capability. Feeds of this type are shown to provide increased efficiency for paraboloidal reflector antennas, improved tracking capability, and simplicity of design.

Author

CONTENTS

CONTENTS (con't)

ILLUSTRATIONS

ILLUSTRATIONS (con't)

ILLUSTRATIONS (con't)

TABLES

A TWO-CHANNEL MONOPULSE REFLECTOR ANTENNA SYSTEM WITH A MULTIMODE LOGARITHMIC SPIRAL FEED

INTRODUCTION

A balanced planar logarithmic spiral (i.e., equiangular spiral) antenna can provide stable impedance and radiation pattern characteristics over extremely wide bandwidths (ref. 1 and 2). A four-arm planar antenna of this type can provide circularly polarized, single lobe, bidirectional radiation on the axis of the antenna. It has been shown that multimode excitations may be used when several log-spiral* arms, with a common origin, are placed on a plane (ref. 3). This simultaneous excitation of two or more field configurations on the same structure, together with techniques for achieving directivity, has been used at Radiation Systems, Incorporated, to design, develop, and fabricate a wideband two-channel monopulse tracking and data-acquisition feed for an 85-foot paraboloidal reflector (ref. 4). This report will enlarge on the theory of multimode log-spiral antennas and describe the operational antenna system which uses this technique.

BACKGROUND

The invention of the balanced equiangular spiral antenna by Turner (ref. 5) in 1952 suggested the concept of a frequency independent antenna to Rumsey (ref. 6,) who first advanced the theory of this device at the University of Illinois in 1954. Du Hamel (ref. 7) immediately extended the theory to include log periodicity of the radiating elements; multimode excitation of logarithmic spiral antennas was first accomplished by Dyson (ref. 8). This theory was reduced to practice at Radiation Systems, Incorporated, where Shelton (ref. 9) and others designed and developed the first planar log spiral, using multimode excitation, to feed a paraboloidal reflector as a two-channel monopulse tracking system.

An opportunity for operational application of the Radiation Systems' log-spiral feed occurred when the TIROS Operational Satellite (TOS) Station was established. This antenna is an 85-foot diameter ground based paraboloidal reflector located at Wallops, Virginia.†

*A convenient abbreviation for logarithmic spiral

†The reflector and X-Y mount for moving it were designed and fabricated by the Rohr Corporation Chula Vista, California, (NAS5-2065) and the system was installed at Wallops, Virginia, by Collins Radio Company, Dallas, Texas (NAS5-2462).

PLANAR LOG-SPIRAL ANTENNA

A log-spiral curve is a plane curve defined in polar coordinates by the equation $\rho = ke^{a\phi}$ as shown in Figure 1; ρ and ϕ being the conventional polar coordinates, a and k being constants. This equation (the expansion ratio) says in effect that the angle of rotation, about some axis D passing through the origin O, must be proportional to the logarithm of the radius vector ρ. The angle α (Figure 1) is a constant and is the angle between the radius vector and a tangent to the log-spiral curve at the point of intersection ($\alpha = \tan^{-1} 1/a$). Because the angle α is a constant, the log spiral is said to be "equiangular". If the angle ϕ is increased by one full turn, the radius vector is increased by the factor $e^{a2\pi}$ hence each turn of the spiral is identical with every other turn except for a constant multiplier. To create an element (arm) of a log-spiral antenna, the edges of the arm (Figure 2) are defined by

$$\rho_1 = ke^{a\phi} \tag{1}$$

and

$$\rho_2 = ke^{a(\phi - \delta)}. \tag{2}$$

The edges of this exponentially expanding arm are identical curves with one rotated, through the fixed angle δ (the arm width), with respect to the other. A second arm may be defined by

$$\rho_3 = ke^{a\left(\phi - \frac{\pi}{2}\right)} \tag{3}$$

and

$$\rho_4 = ke^{a\left(\phi - \frac{\pi}{2} - \delta\right)}. \tag{4}$$

This arm, identical to the first arm, has a point of origin 90 degrees from the first. Remaining arms of a multiarm structure may be defined by rotating curves (1) and (2) through π/N radians, and in this manner the four-arm log-spiral antenna (Figure 2) was constructed. The figure shows the spiral broken which was necessary in designing the dual spiral feed for the TOS antenna. The radius vector from the origin O to an inner feed circle is denoted by ρ_o; the radius vector to an outer feed circle is denoted by ρ_m. Du Hamel (ref. 10) recognized that such an antenna could be completely specified by the angle δ which determines the arm width and the constants a and k, the former defining the rate of spiral and the latter the size of the terminal region.

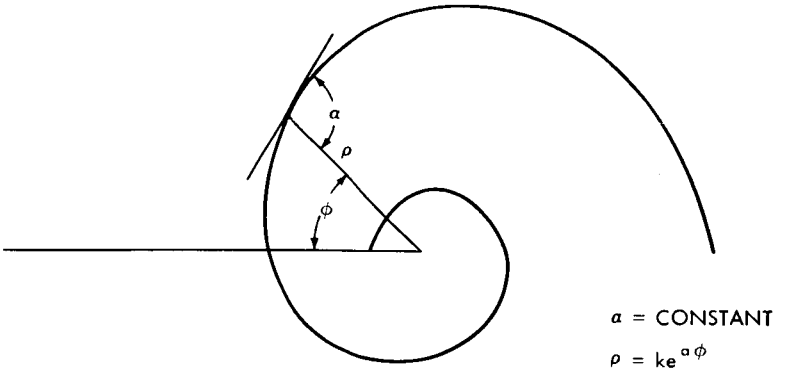

Figure 1. Log Spiral Curve

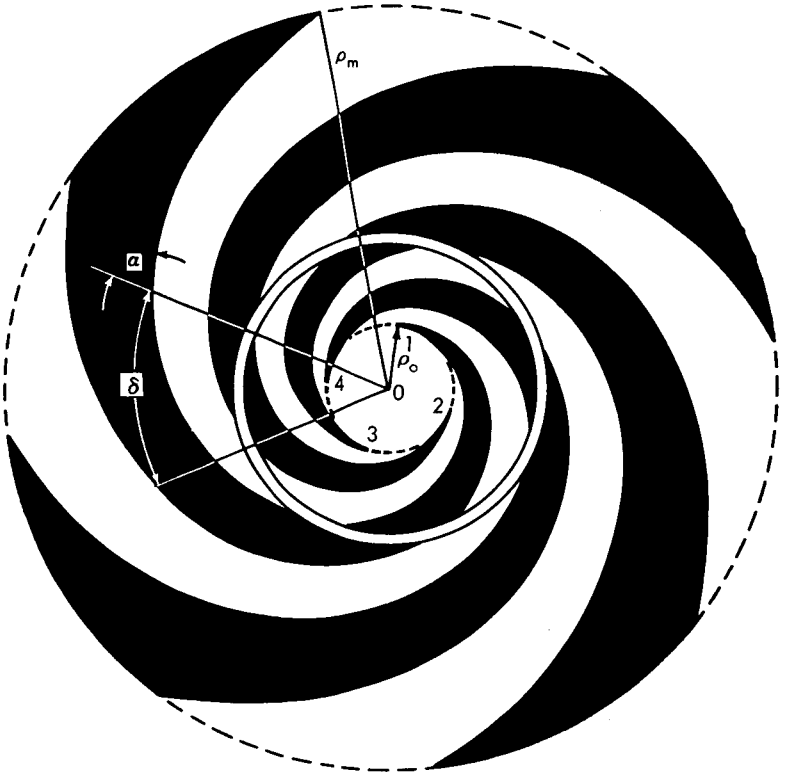

	INNER SPIRAL	OUTER SPIRAL
ρ_o	0.531"	12.375"
ρ_m	11.875"	42.250"
δ	45°	45°
α	86°	86°

Figure 2. Stylized Sketch of Dual Four-Arm Planar Log Spiral Showing Defining Parameters

MODAL EXCITATION OF MULTIARM LOG SPIRALS

A detailed explanation of modal excitation on multiarm log spirals by Kaiser (ref. 11) presents the spiral as a two-wire transmission line gradually transforming into a radiating structure.

According to Kaiser, the currents on a two-wire transmission line are out-of-phase at any normal cross section, hence radiation does not occur. As previously stated, the arms of a four-arm spiral are identical (could be superimposed) but are rotated about the spiral axis so that the input terminal points are 90 degrees apart. In a two-arm spiral, one arm is rotated 180 degrees relative to the other. In a two-arm spiral, one can progress along one arm around to a point exactly $\lambda/2$ along a circular arc away from a corresponding point lying on the other arm; both points are contained in a common circle centered on the spiral axis. Difference in line lengths from the input terminals to a point on adjacent elements is πr and circumference at this point is $2\pi r$, where r is the radius from the center. Currents are in-phase on adjacent filaments at a one-wavelength circumference (if the two-arm spiral is fed out of phase) and radiation occurs. This region of radiation is called the first mode region. When a circumference of $2\pi r$ equals λ, then the radius to the circle where the first mode radiates with maximum intensity is $r = \lambda/2\pi$. Currents existing beyond the one-wavelength ring will continue experiencing phase change as they progress outward, and at each in-phase location, subsequent areas (modes) of radiation will occur.

If the input arms are fed in-phase, little radiation occurs at the feed point because of the close spacing; however, at the proper distance from the center (as previously described) an in-phase condition will again occur which does set up radiation. In general, feeding out-of-phase will set up the odd numbered modes (i.e., 1, 3, and 5, etc.) while feeding in-phase will set up the even numbered modes (i.e., 2, 4, and 6, etc.).

The extremities of the active region across the face of a log spiral, in which each mode is active, were measured by Ransom (ref. 12) by probing. Figure 3 shows a plot of typical modal excitations. It can be seen that the areas over which modes are measurable overlap and that peak intensities occur at $\lambda/2\pi$, λ/π, and $3\lambda/2\pi$ as would be expected for modes 1, 2, and 3. The need can be seen for a mode suppressor, over part of the spiral edge, to clear up the third mode if it is not wanted (i.e., for acquisition or other purposes).

These basic excitations of multiarm log-spiral antennas give rise to radiated fields with azimuthal variations of the form $e^{\pm jm\phi}$. The excitation of a four-arm log-spiral antenna will produce modes with integer values of m as $m = 1, 2,$

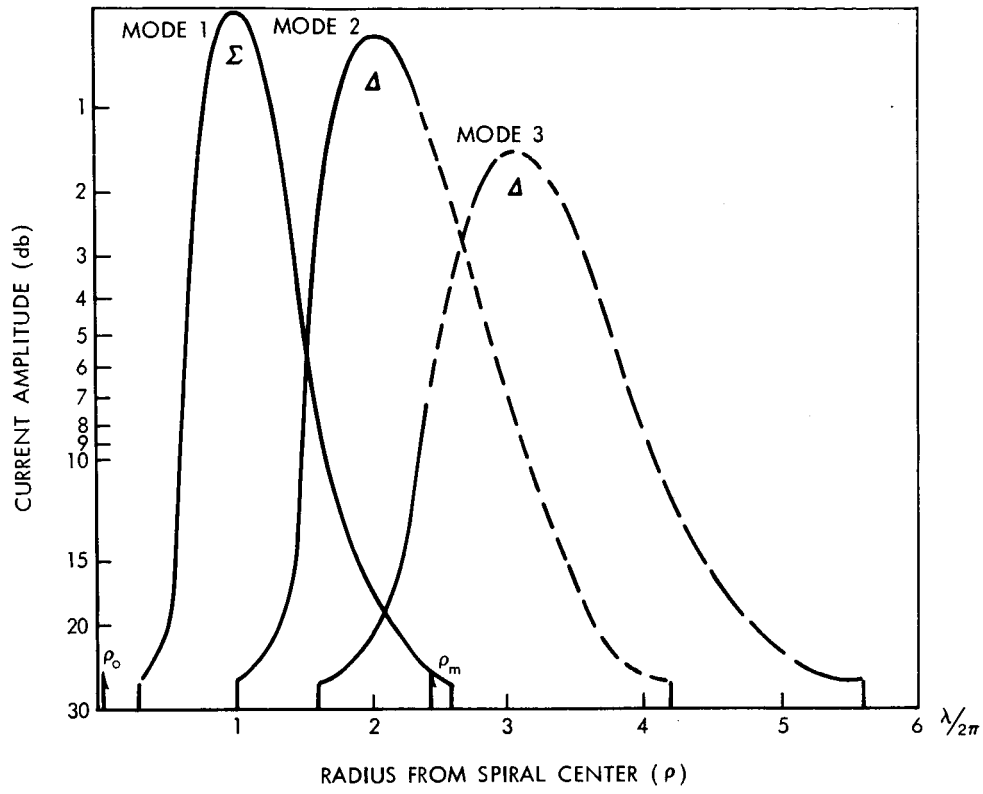

Figure 3. Typical Reactive Near-Field Modal Excitation Across a Four-Arm Log Spiral, $\alpha = 86°$

and 3. It can be shown that an N-arm spiral can support N-1 modes of excitation. Recalling that $e^{j\phi} = \cos\phi + j \sin\phi$, these excitations can be determined for a left-hand wound four-arm spiral to be:

when

$$m = 1, \quad A_1 = (1, j, -1, -j)$$

$$m = 2, \quad A_2 = (1, -1, 1, -1)$$

$$m = 3, \quad A_3 = (1, -j, -1, j)$$

where A_n is the current vector notation for the excitations at the four input terminals, and the input terminals are numbered in the counterclockwise direction around the feed circle. When $m = 1$, the field pattern $e^{j\phi}$ is an axial beam directed both ways along the axis and normal to the plane of the spiral. (Cavity backing or other techniques direct energy for feeding a reflector.) When $m = 2$ or 3, the field patterns $e^{j2\phi}$ and $e^{j3\phi}$ are conical fields (null on the axis). These modes are used to obtain difference patterns for monopulse applications.

Radiated fields are circularly symmetric about the spiral axis with no variation in phase contours if the circularity is pure.

In keeping with the Institute of Electrical and Electronics Engineers (IEEE) standard (ref. 13), the polarization sense of the log-spiral antenna may be determined from the hand used when pointing the fingers in the direction of the spiraled arm currents and the thumb in the direction of the radiated fields. Since the currents are assumed to travel away from the feed terminal, right-hand circular polarization corresponds to phase delay in the direction of increasing ϕ in the positive half-space; left-hand circular polarization corresponds to phase advance in the direction of increasing ϕ. Consequently, center-fed spiral antennas wound in the right-hand sense, as in Figure 2, will produce primary fields with phase variation of the form $e^{-jm\phi}$ and those wound in the left-hand sense would produce fields with phase variation $e^{+jm\phi}$ (viewing the radiation going away from the observer). Notice that in any case m must be an integer for the field to be single valued. Moreover, the sense of circularity is reversed on return from a paraboloidal reflector so that the sense of secondary patterns is the opposite of that described for primary fields.

The phase of the $m = 1$ mode is extremely well behaved. This may be associated with the purity of the excitation because it is easy to feed the arms in this mode, i.e., opposite arms are connected at the apex and the connected pairs are fed in phase opposition. The $m = 2$ mode requires additional phase shift in the feed lines as shown in Figure 4.

Typical radiation patterns of a four-arm log-spiral antenna excited in the three modes are shown in Figure 5. The rate of spiral growth (the parameter α) determines the shape of the conical beam of the balanced four-arm antenna. The spread of the difference pattern lobes (on secondary reflection) increases with mode number, providing wide-angle acquisition capability for a monopulse search antenna system.

TIROS OPERATIONAL SATELLITE (TOS) ANTENNA REQUIREMENTS

The command and data-acquisition (CDA) station at Wallops, Virginia is part of the National Operational Meterological Satellite System. This station tracks, commands, and acquires data from meterological satellites in the TOS system, and supplements a similar antenna station at Fairbanks, Alaska. The TOS-Wallops station was built by the Goddard Space Flight Center and is operated by the Environmental Science Services Administration.

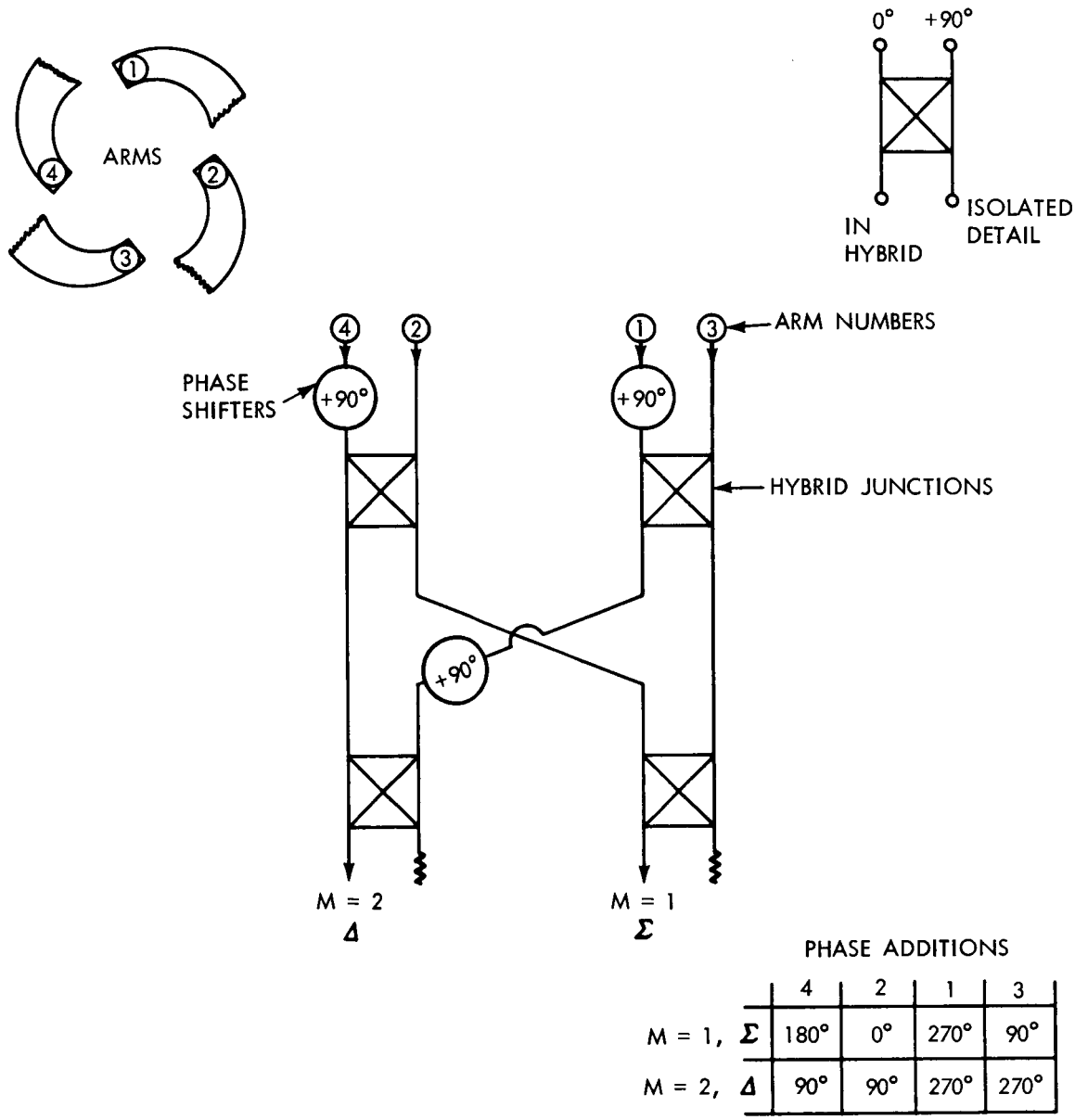

PHASE ADDITIONS

	4	2	1	3
M = 1, Σ	180°	0°	270°	90°
M = 2, Δ	90°	90°	270°	270°

Figure 4. Excitation Network for Four-Arm Log Spiral

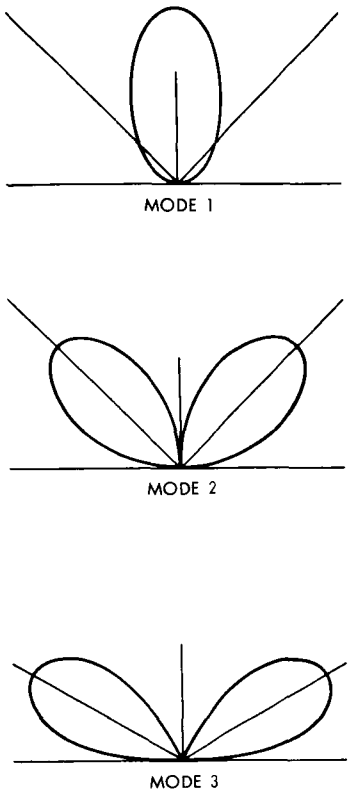

Figure 5. Typical Radiation Patterns of a Four-Arm Log-Spiral Antenna for each Excitation Mode

The ground-based antenna at the TOS-Wallops station is an 85-foot diameter, X-Y mounted paraboloidal reflector ($f/D = 0.42$) antenna with a focal-point feed. The antenna must now be capable of acquiring and tracking data at 136 and 235 Mc with capability for later operation at frequencies near 400 Mc and subsequently at higher frequencies. Autotrack operation in both senses of circular polarization is required. For telemetry reception, it is required that both senses of circular polarization be received simultaneously with no switching.

REFLECTOR FEED

Choice of Feed Type

In the past, prime focus monopulse feeds for National Aeronautics and Space Administration (NASA) reflector antennas have used crossed dipoles over a reflecting screen. Four crossed dipoles for each frequency of operation provide sum and difference pattern illumination when used with an appropriate RF monopulse feeding network. Feeds were designed in this manner because their performance characteristics were well known, they were light, and they were economical to construct. Performance capability of a reflector fed in this manner is somewhat limited, particularly as the number of frequency bands which must be covered (and hence, groups of crossed dipoles required) increases. These limitations are discussed in the Appendix. The planar multiarm log periodic spiral feed was selected because it offers advantages over these limitations. These advantages are discussed in the same order as topics discussed in the Appendix to facilitate comparison.

The primary pattern of a log spiral has true circular symmetry and is ideal for illuminating a reflector with a circular aperture. Edge illumination can be precisely controlled; therefore, antenna temperature, sidelobes, gain, and efficiency can be optimized. The difference mode of excitation (mode 2) is excited at a diameter on the planar spiral which is exactly twice the diameter at which the sum mode (mode 1) is excited. As a consequence, the primary difference aperture is twice as large as the sum aperture and the primary difference pattern falls entirely inside the envelope of the primary sum pattern main lobe. This situation permits optimum reflector edge illumination for the sum as well

as for the difference patterns. Tracking error is reduced because secondary difference pattern sidelobes are reduced from 18 db for a dipole feed to 30 db for the log-spiral feed as shown later by measured and computed patterns. Noise temperature (at 1700 Mc) can be shown to be reduced from 75° K for the dipole feed to 40.5° K for the optimized log-spiral feed.

NOTE

Antenna noise temperature is discussed at 1700 Mc because sky noise at 136, 235, or 400 Mc is so high that the contribution due to the antenna alone is meaningless.

This temperature reduction is substantiated by measurements (ref. 14) of temperature of an 85-foot reflector with dipole feed and by computations by Hansen (ref. 15) for optimum aperture illumination. Extrapolating Hansen's data for 1700 Mc (Table 1) indicates antenna temperature when a planar log-spiral fed antenna is directed toward quiet sky. No extrapolation is made for 235 Mc because at this frequency atmospheric noise (ref. 16) is 370° K and far exceeds noise due to aperture efficiency.

Table 1

Anticipated Antenna Temperature for Log Spiral Reflector
Pointed at Quiet Sky at 1700 Mc
(°K)

Main beam and upper sidelobes, Gain = 0.82 = 0.075 = 0.895	
Atmospheric absorption = 0.021; ambient = 290; 0.895 × 0.021 × 290 =	6.0
Galactic absorption = 0.979; ambient = 15; 0.895 × 0.979 × 15 =	13.4
Lower sidelobes, Gain = 0.075	
Ground absorption = 0.500; ambient = 290; 0.075 × 0.500 × 290 =	10.9
Atmospheric absorption = 0.021; ambient = 290; 0.075 × 0.021 × 15 =	0.4
Galactic absorption = 0.979; ambient = 15; 0.075 × 0.979 × 15 =	1.1
	31.8
3% heat loss - 0.03 × 290 =	8.7
Total temperature	= 40.5

Because of the circular symmetry, antenna aperture efficiency is increased from 39 percent for the dipole feed to 65 percent for the planar log-spiral feed. This results in a direct 2.2-db increase in gain over the dipole feed. Figure 6 illustrates the elliptical primary difference lobes of a dipole feed impinging on the prime reflector and compares this situation with the circular contours of equal power that impinge on the reflector when a planar log-spiral feed is used. This situation is a result of circular symmetry of the prime difference pattern of a log spiral. Reduction of spillover loss for the log-spiral feed is made obvious by Figure 6. The 39 percent efficiency for the dipole feed is derived in the Appendix and the 65 percent efficiency for the log-spiral feed is derived comparing measured log-spiral primary patterns with primary pattern shapes analyzed by Sciambi (ref. 17) to compute efficiency from a circular aperture.

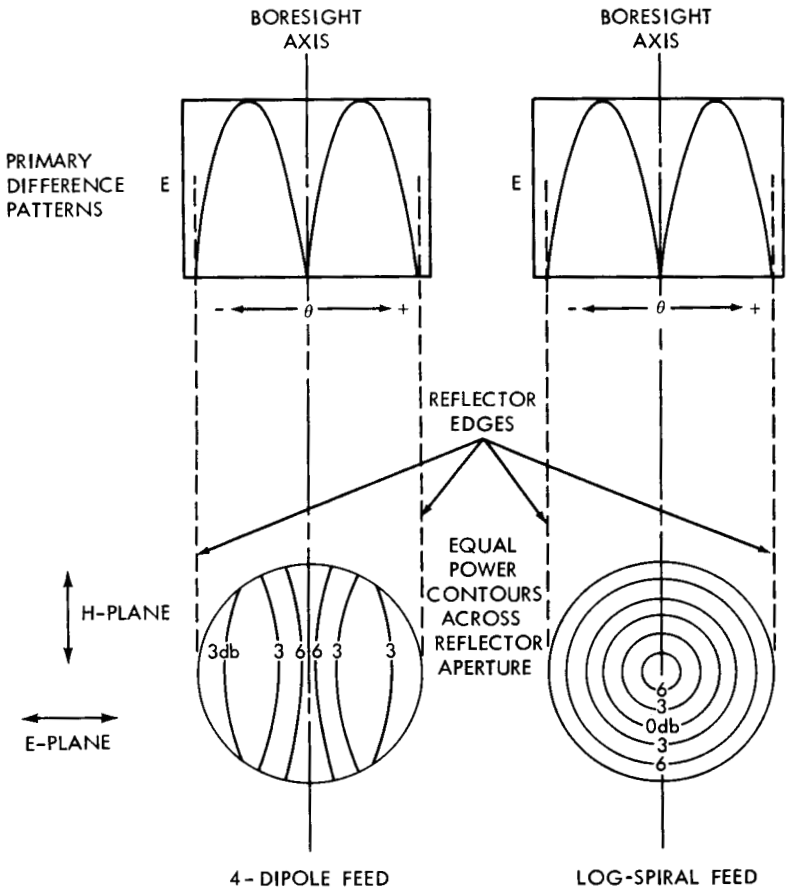

Figure 6. Comparison of Reflector Illumination Contours Assuming Equal Difference Patterns for Dipole and Log-Spiral Feeds

Measured tracking error of a STADAN dipole-fed paraboloidal reflector antenna is tabulated in the Appendix for various frequencies. This error can be extrapolated to be ±5 milliradians at 235 Mc, and is largely due to inability to construct a dipole feed with perfect mechanical symmetry, as well as inability to cut and maintain RF feed lines with no phase error. When photoetching is used to form the copper spiral arms, construction of a planar log-spiral feed is limited only by drawing accuracy. The boresight error of a planar log-spiral feed was determined (ref. 18) to be ±2 milliradians. This is a substantial improvement over dipole feeds and is a result of accuracy in photoetch forming the feed, printed circuit RF feedlines and hybrid junctions, and reduced RF line lengths. In consideration of all of the above findings, the planar log-spiral feed was initially installed in the TOS-Wallops reflector antenna.

Spiral

To establish the optimum design of the spiral, three experimental models (scale 2.5:1) were constructed having a rate of spiral growth (angle α , Figure 2) equal to 84.5, 86.0, and 87.5 degrees. Current distribution across each spiral model, as well as the pattern performance, was measured. It was determined that the loosely wound spiral ($\alpha = 87.5°$) resulted in a large feed structure with attendant excessive aperture blocking. The tightly wound spiral produced a pattern with excessive beamwidth resulting in high edge illumination on the reflector. Dyson (ref. 2) has shown that the parameter α is the primary factor in controlling the beamwidth of the planar log-spiral antenna. The spiral with an 86-degree angle of wrap was selected as optimum. A copper film, deposited on glass cloth laminate (MIL Spec. NEMA G-10), was etched to form the filament windings. Current distribution across this spiral is shown in Figure 7. This data is extrapolated from measurements on the 2.5:1-scale model and is plotted against the full-scale spiral radius dimensions. The significance of the terms "inner spiral" and "outer spiral" which appear in Figure 7 is explained in the following section.

Cavity Reflector

To direct the feed pattern onto the reflector, it was necessary to back the spiral with a cavity. Because a cavity is a frequency-sensitive device, a single cavity could not provide optimum operation over the entire 136- to 406-Mc frequency band; hence, two concentric cavities were used. The inner cavity is a solid metallic can 6.214 inches deep which backs a spiral recessed 1 inch below the outer spiral. The outer cavity, backing the outer spiral, is also a solid metallic can 17.126 inches deep. No dielectric loading was used in either cavity although some styrofoam egg-crate structure is used in the outer cavity for mechanical support. Therefore, the outer cavity is 0.195 λ deep at 136.5 Mc and

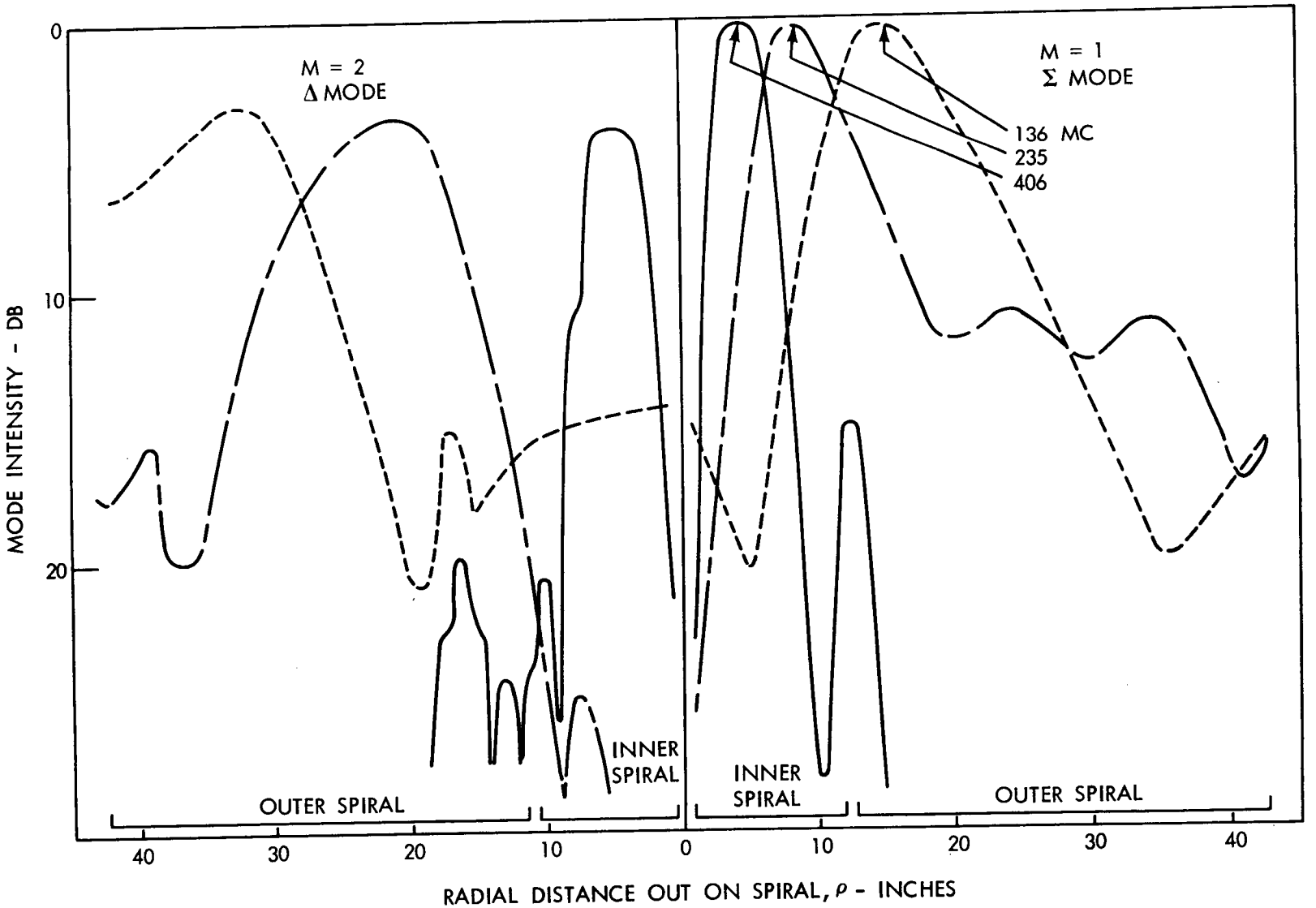

Figure 7. Distribution of Modal Excitation Across Spiral

0.341 λ deep at 235 Mc. The spiral over this cavity supports the sum and difference modes at 136.5 Mc and the difference mode at 235 Mc. The inner cavity is 0.124 λ deep at 235 Mc and 0.214 λ deep at 406 Mc. The spiral over this cavity supports the sum mode at 235 Mc and the sum and difference modes at 406 Mc. Figure 7 shows that the desired modal distribution was achieved. Figure 8 is a graphic illustration of the relationship of cavities and spirals showing pertinent dimensions.

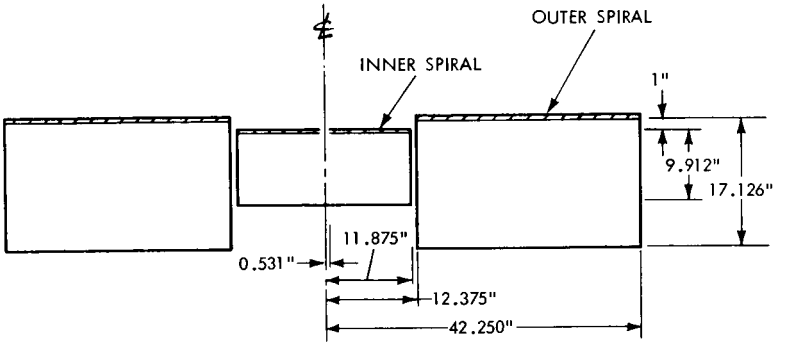

Figure 8. Cavity Arrangement

Theoretical Phase Center

The phase center (center of equal-phase contours) of the planar log-spiral antenna is derived in a theoretical analysis by Cheo, Runsey, and Welch (ref. 19). These investigators considered only the spiral in free space and determined that the phase center is located behind the spiral for an observer located on the spiral axis of symmetry. The distance h behind the spiral to the phase center is a phase function of the angle of the observer off axis θ and the wavelength. The authors point out that

$$\frac{h}{\lambda} = \frac{\psi(\theta)}{2\pi \cos \theta} , \tag{5}$$

assuming there is no lateral displacement; that is, the phase center is on the axis of symmetry. For tightly wound spirals, i.e. α = 60 to 90°, (5) is approximately

$$\frac{h}{\lambda} = \frac{a}{2\pi} \tag{6}$$

where the angle of wrap $\alpha = \tan^{-1} \frac{1}{a}$.

Dyson (ref. 20) confirmed this theoretical determination by measuring centers of phase of planar log spirals. He found that for most practical spirals the phase center is approximately

$$\frac{h}{\lambda} = \frac{a}{2\pi} + 0.02 , \tag{7}$$

for all modes of excitation. Dyson provided curves for correcting (5) which indicate that for a spiral in which $\alpha = 86$ degrees the correction to (5) for the sum mode $m = 1$ is $0.002\,\lambda$, and for the difference mode $m = 2$, the correction is $0.039\,\lambda$. Hence, it can be expected that the phase centers would lie behind the spirals and that

$$h = \left(\frac{a}{2\pi}\right)\lambda + 0.002\lambda, \quad \text{for } m = 1$$

and (8)

$$h = \left(\frac{a}{2\pi}\right)\lambda + 0.039\lambda, \quad \text{for } m = 2$$

Substituting the values for a ($a = 0.07$ for $\alpha = 86$ degrees) and λ ($\lambda = 87.6$ inches at 136.5 Mc and 50.2 inches at 235 Mc) in equation (8) indicates that at 136.5 Mc the phase centers should be 1.14 inches behind the spiral for the sum mode and 1.30 inches behind the spiral for the difference mode. At 235 Mc, the same parameters are 0.65 inches and 0.74 inches, respectively. It can be seen that to coalign the average phase center locations for $m = 1$ and $m = 2$, it is necessary to recess the inner spiral 0.7 inches ($0.008\,\lambda$ at 136 Mc and $0.013\,\lambda$ at 235 Mc). No phase centers have been measured in the presence of a cavity backing. It is assumed that the cavity will move the phase center toward the spiral. In consideration of this lack of information, the high-frequency spiral was recessed 1 inch behind the outer low-frequency spiral.

The lateral displacement of phase centers is of interest in order to properly locate a spiral feed in a reflector antenna. Dyson (ref. 20) measured this parameter for one two-arm planar log spiral and found it to be remarkably close to the axis of symmetry for the sum mode. Cursory measurements of the phase center location of a scale model 1700-Mc planar log spiral at the Goddard Space Flight Center indicated the location to be 0.25 inch behind the spiral and so close to the axis of symmetry that a lateral displacement, if any existed, could not be measured.

Impedance Matching

The four-arm planar spiral antenna is a symmetrical structure and, when excited in a balanced manner, radiates a beam on the axis of symmetry without squint or tilt. A tilt in the radiation pattern can always be traced to the physical construction, to unbalance in the excitation network, or to coupling effects. This antenna is excited in the balanced condition in the sense that opposite windings

are 180 degrees out of phase. The conversion from unbalanced coaxial line to the balanced condition takes place in printed-circuit (180-degree) hybrids and phase shifters in four printed-circuit matrices, one each of which is associated with the inner or outer terminals of each spiral. The excitation network is discussed in a later section of this report.

Impedance transformation from the 50-ohm characteristic impedance of the coaxial feed line to the 135-ohm impedance at terminal points of windings takes place in a three-fold matching network. The outer ends of outer spirals are fed with: (1) rigid, teflon-filled coaxial line, (2) a section of microstrip line, and (3) a section of continually expanding filament winding. This matching network is used at both the outer and inner terminals of the outer spiral, and the coaxial line transformer is cut to be $\lambda/4$ long at 136.5 Mc. The outer terminals of the inner spiral are fed in the same way, with the coaxial transformers cut to be $\lambda/4$ at 406 Mc. Inner terminals of the inner spiral are fed directly with 50-ohm coaxial line. A paper by Wheeler (ref. 21) contains an excellent discussion of the effects of unbalance in the excitation of log-spiral antennas.

TWO-CHANNEL MONOPULSE SYSTEM

RF System

The TIROS Operational Satellite (TOS) command and data-acquisition (CDA) station at Wallops, Virginia, described earlier in this report, uses a two-channel RF system for following a satellite and acquiring telemetry with an 85-foot reflector antenna. The planar log-spiral feed previously described was specifically planned for potential use with this antenna system. Description of the complete RF system is included to provide a comprehensive picture and to facilitate discussion of feed performance characteristics.

Figure 9 is a three-part schematic of the RF system. Terminal ports, associated with each spiral filament winding, are connected to four printed-circuit matrices by RG-115A/U flexible coaxial cable. Each matrix consists of four hybrid couplers and three 90-degree phase shifters. (Matrices are described in detail in the following section.) One matrix each is associated with the outer and inner terminals of the outer and inner spirals; thereby, two matrices process right circular polarized signals and two process left circular polarized signals. A sum and a difference signal are derived from each matrix. Matrices are connected to frequency diplexers and to preamplifiers by RG-254/U "Spiraline" RF cable. Diplexers, described in the following section, are constructed using printed-circuit techniques. Channels for operation at 406 Mc are closed off in Figure 9 because this frequency is planned for future implementation.

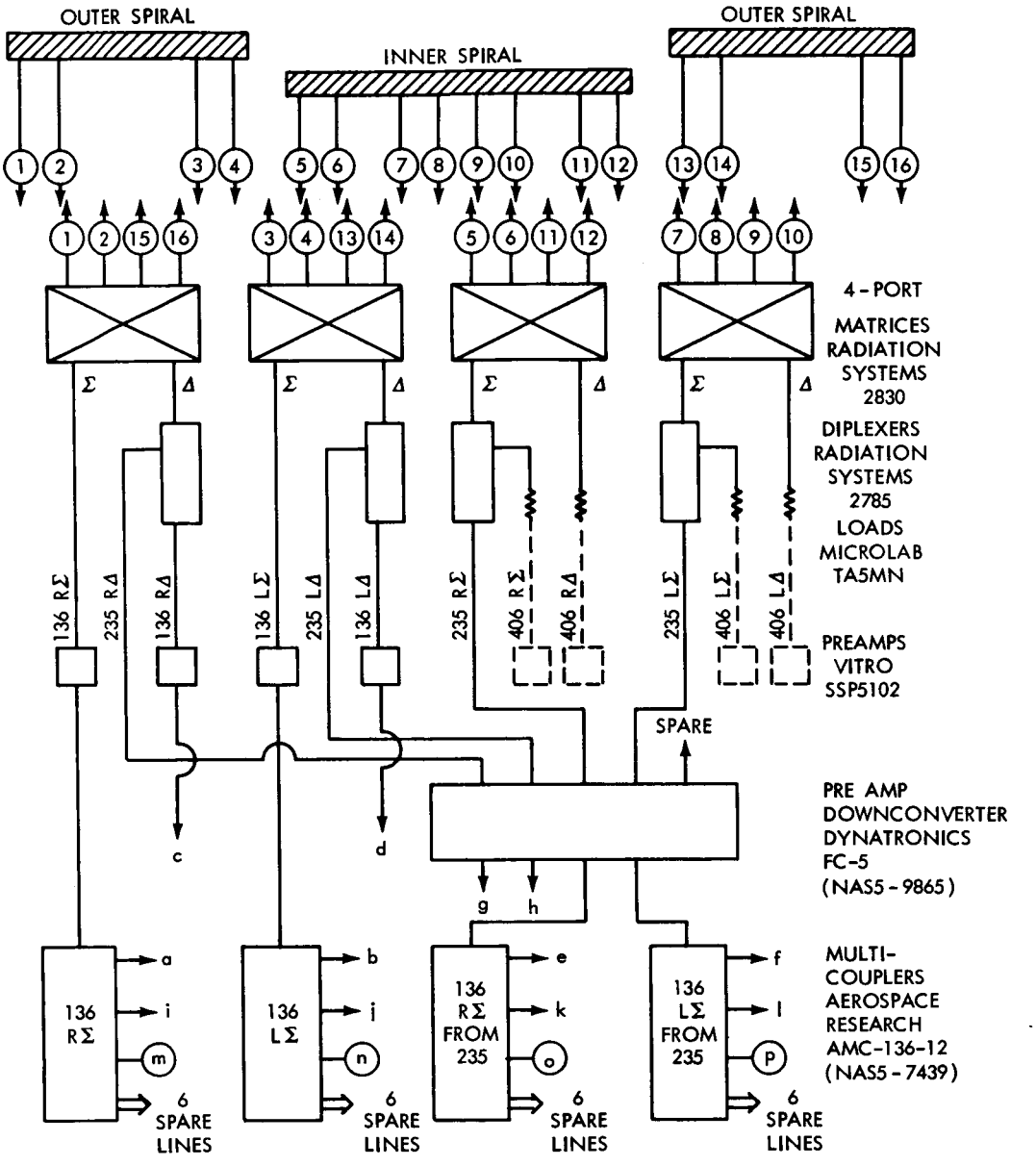

Figure 9. TOS-Wallops Antenna RF System

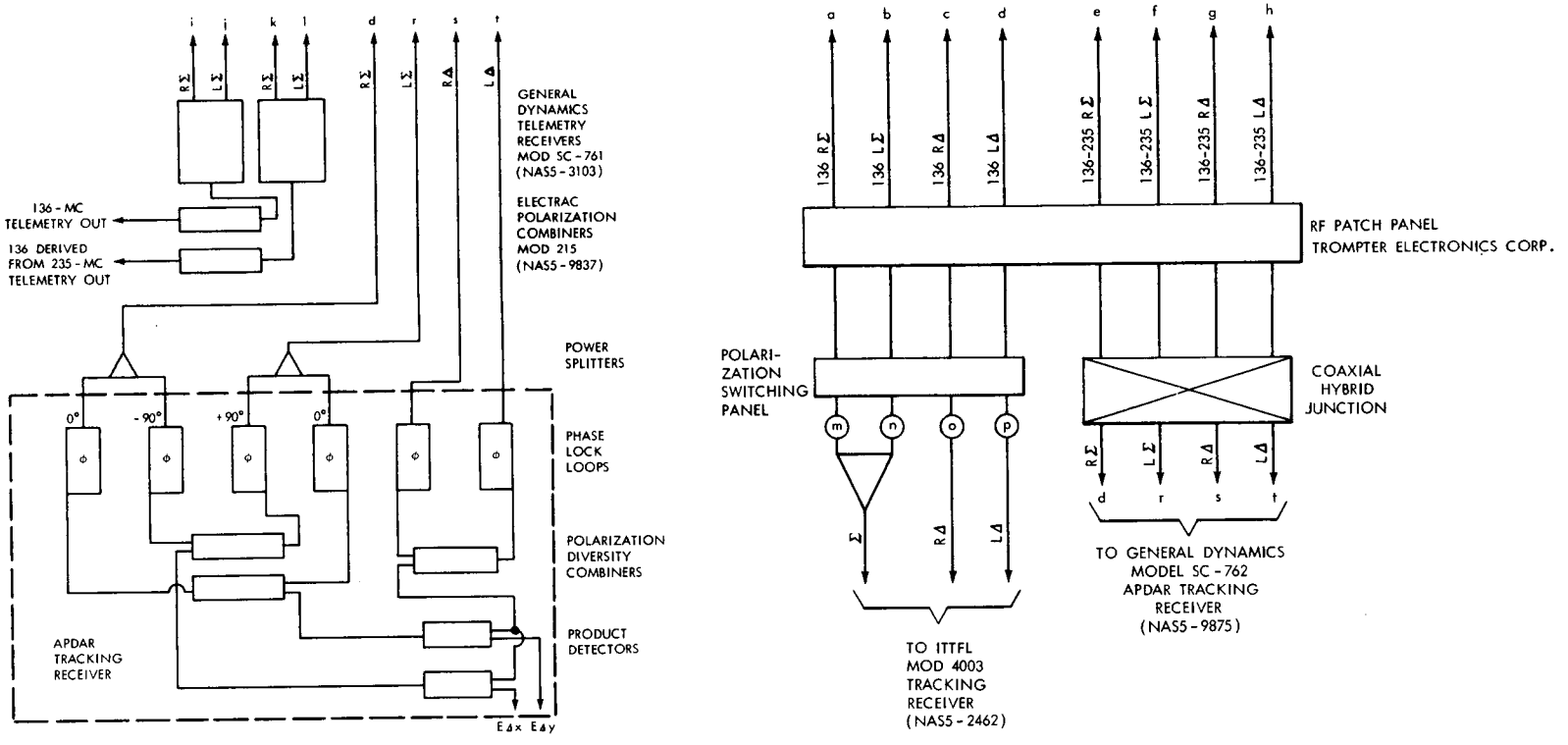

Figure 9. TOS-Wallops Antenna RF System

Figure 9 shows model numbers and procurement contract numbers for proprietary parts. A combination preamplifier and frequency down converter reduces the 235-Mc signal to 136.5 Mc. Multicouplers, a coaxial line patchpanel, and coaxial hybrid junctions are used as required to adapt to the receivers. Telemetry is received with two General Dynamics SC-761 receivers. Electrac 215 polarization combiners are required to carry both senses of circular polarization on single lines at 136.5 and 235 Mc. An International Telephone and Telegraph Federal Laboratories (ITTFL) 4003 and a General Dynamics SC-762 receiver provide tracking capability at 136.5 and 235 Mc respectively. Simultaneous tracking on either sense of circular polarization is accomplished with minimum RF-line hybrid junction loss and no RF-line switches. Polarization diversity combining is achieved in the General Dynamics receiver.

Excitation Network

The network used to excite the planar log-spiral feed produces the phase progressions on filament windings as shown in Figure 10. For the sum mode of

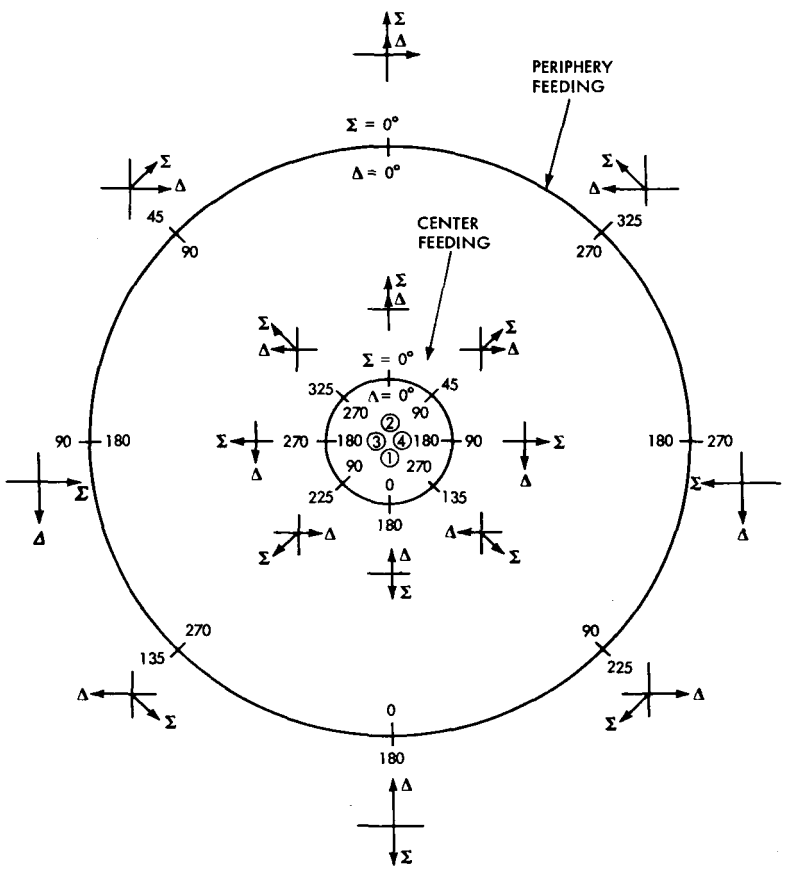

Figure 10. Phase Relationships Between First (Σ) Mode and Second (Δ) Mode for Right-Circular Wound Spiral

operation for left-circular polarization (after reflector reversal) the spiral arms are excited at the inner ends of filaments with a phase progression of 0, -90, -180, and -270 degrees. Likewise, for right-circular polarization of the sum mode, the spiral is excited at the outer ends of filament windings. For difference mode excitation, the spiral filaments are excited with a phase progression of 0, -180, -360, and -540 degrees. Vector relationships for sum and difference mode excitations are indicated on Figure 10. To produce these phase progressions, stripline matrices were designed and developed. Each matrix is composed of quadrature couplers and 90-degree phase shifters. Figure 11, a block diagram of a matrix, shows a detailed schematic of the hybrid junction coupler used in the matrix. Amplitudes through the four-port hybrid junction are in 1:1 relationship. Figure 12 is a plot showing the isolation, coupling unbalance, and VSWR of the hybrid junction component. Figure 13 shows the characteristics of the 90-degree phase shifter used in each matrix. Characteristic performance of the complete matrix at 136.5, 235, and 406 Mc is read from the curves of Figures 12 and 13 and is listed in Table 2. Figure 14 is a schematic

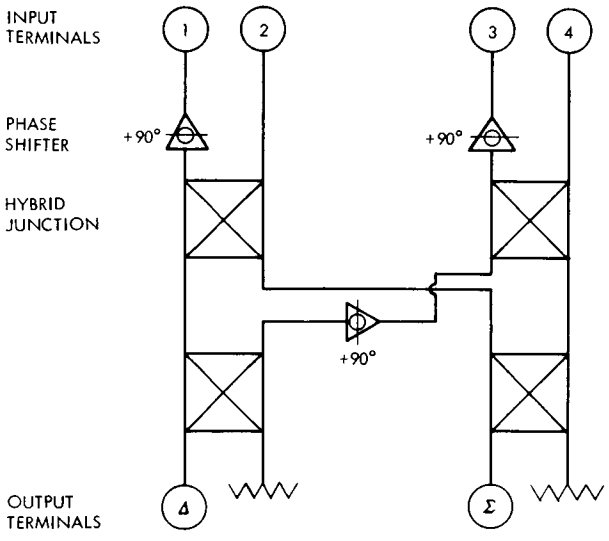

OUTPUT TERMINALS	INPUT TERMINALS			
	1	2	3	4
Σ	180°	0°	270°	90°
Δ	90	90	270	270

MATRIX TERMINAL PHASE RELATIONSHIP

Figure 11. Typical Excitation Matrix, Block Diagram

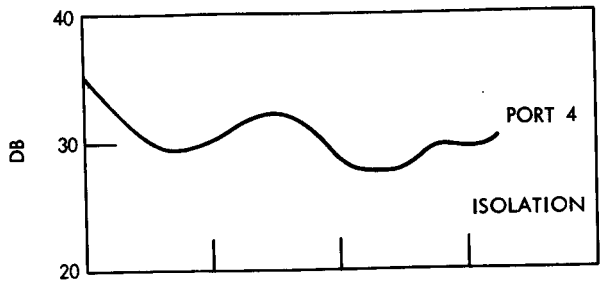

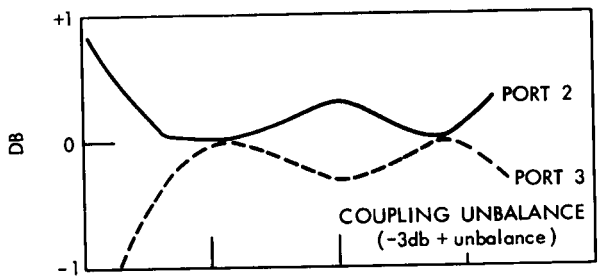

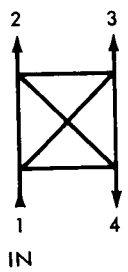

Figure 12. Performance of Printed-Circuit Hybrid Junctions.

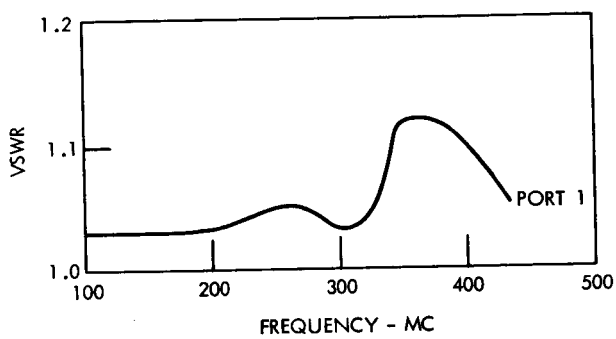

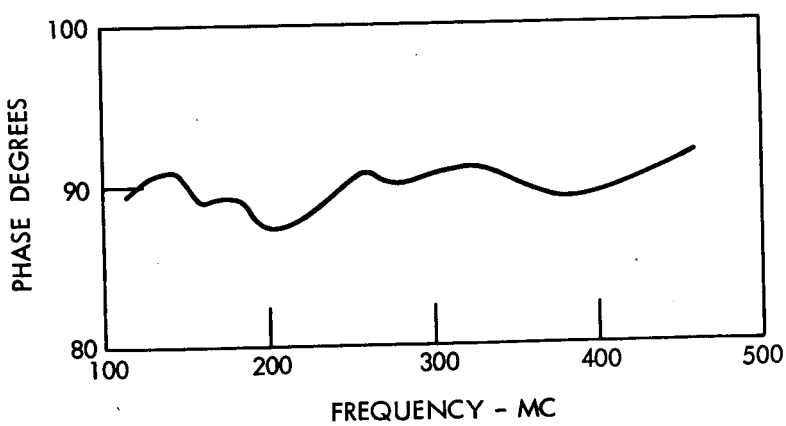

Figure 13. Performance of 90-Degree Phase Shifter.

of the printed circuit deplexers; performance characteristics of these units are plotted in Figure 15.

Table 2

Performance Characteristics of Printed-Circuit RF Matrix

Freq. (Mc)	Mode	VSWR	Amplitude Unbalance (db)	Phase Error (degrees)	Isolation (db)
136.5	Σ	1.07	± 0.35	± 3.0	43
136.5	Δ	1.08	0.30	3.5	—
235	Σ	1.02	0.30	9.0	35
235	Δ	1.03	0.10	1.0	—
406	Σ	1.10	0.20	5.0	30
406	Δ	1.11	0.10	5.5	—

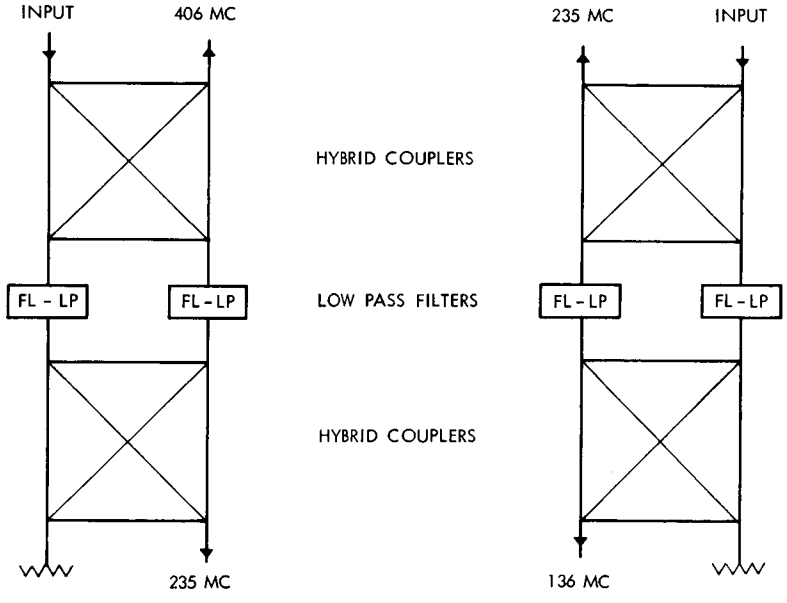

Figure 14. Printed-Circuit Diplexers, Schematic

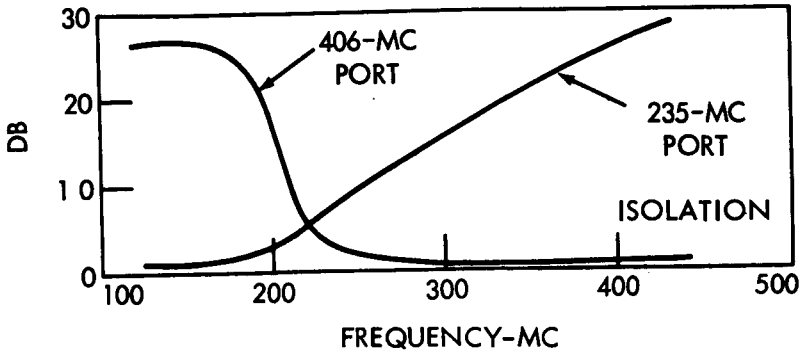

235/406 MC
DIPLEXER

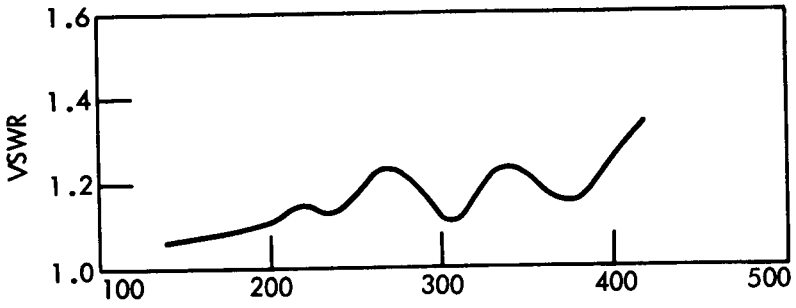

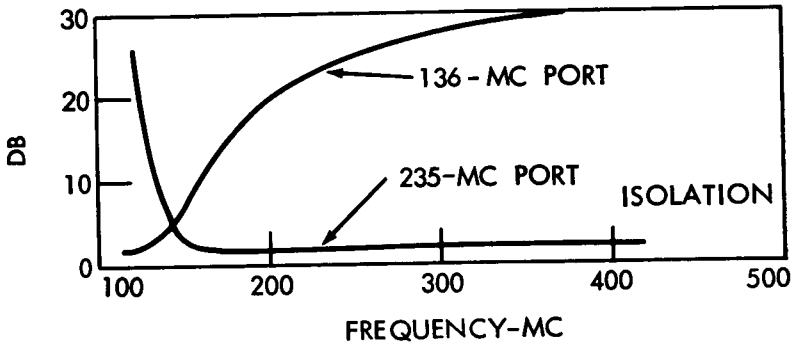

136/235 MC
DIPLEXER

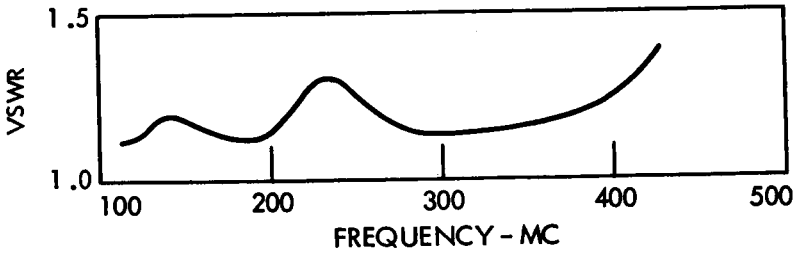

Figure 15. Performance of Printed-Circuit Diplexers

ANTENNA PERFORMANCE RESULTS

Primary Patterns

Primary patterns were measured by locating a field-generating antenna (crossed log-periodic dipole structure) beyond the Fresnel-Fraunhofer boundry. This antenna was, in fact, 51 feet away from the planar log-spiral antenna which was mounted on a standard elevation over azimuth pedestal. Figure 16 is a photograph of the 2.5:1-scale model feed; Figure 17 shows the full-scale feed with all the RF printed-circuit boards. Figures 18, 19, and 20 show the primary patterns at 136.5 Mc, 235 Mc, and 406 Mc, respectively. It can be seen that for the most part the difference patterns ($m = 2$) are within the envelope of the sum pattern ($m = 1$) and average edge illumination for both modes is approximately equal. Table 3 lists average (average of illumination on both sides of the reflector) edge illumination for both modes and polarization senses. The

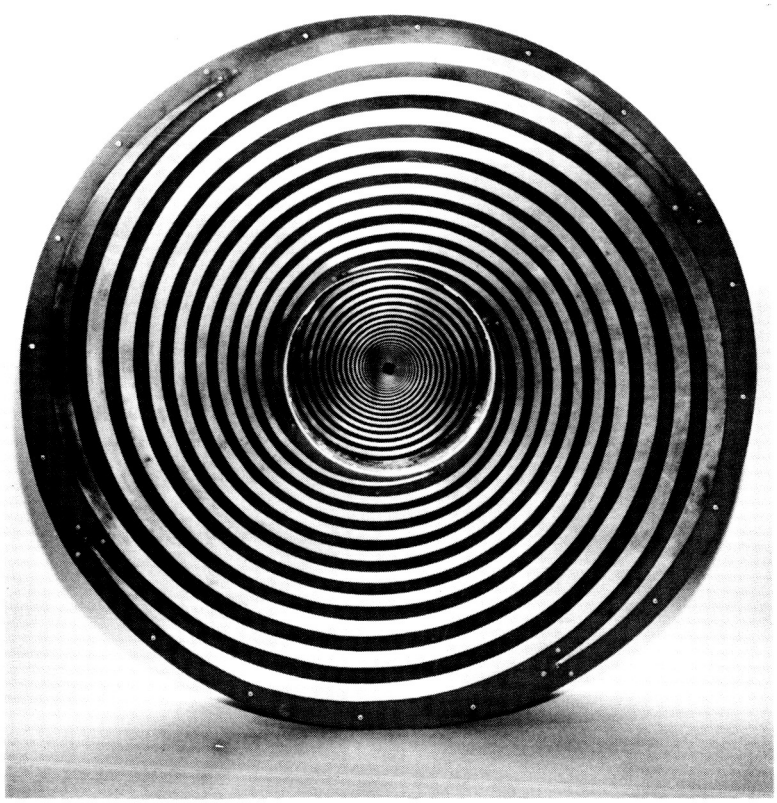

Figure 16. 2.5:1-Scale Model of Feed

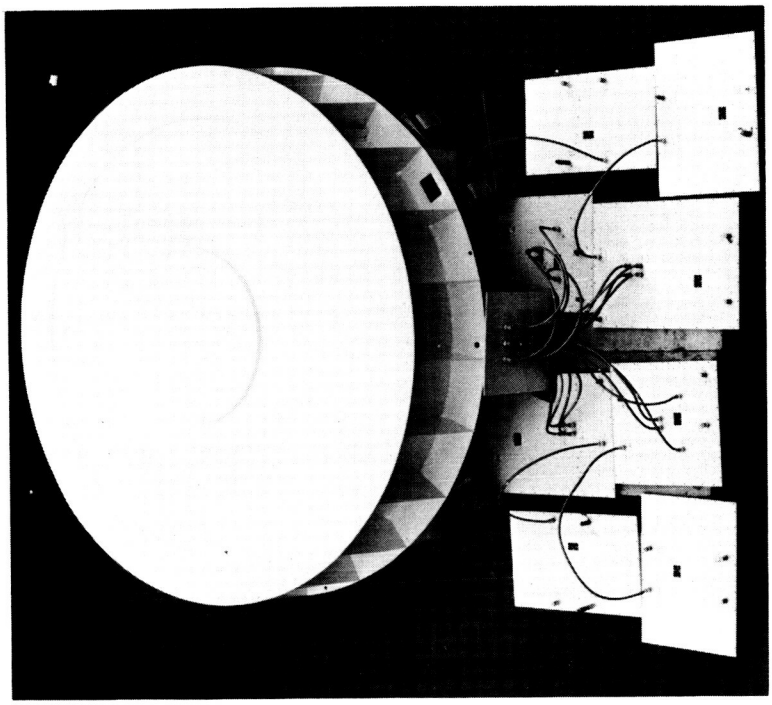

Figure 17. Full-Scale Feed with all RF Printed-Circuit Boards

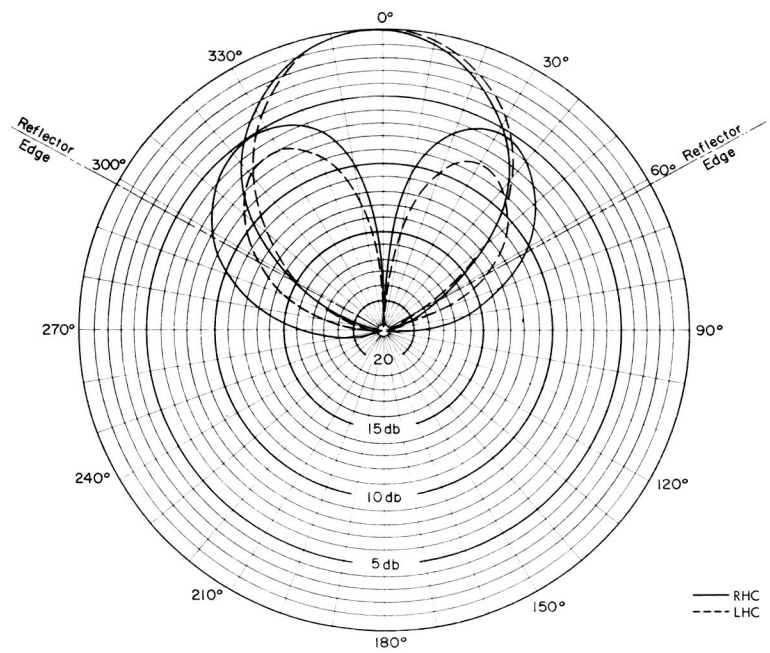

Figure 18. Primary Pattern-136.5 Mc

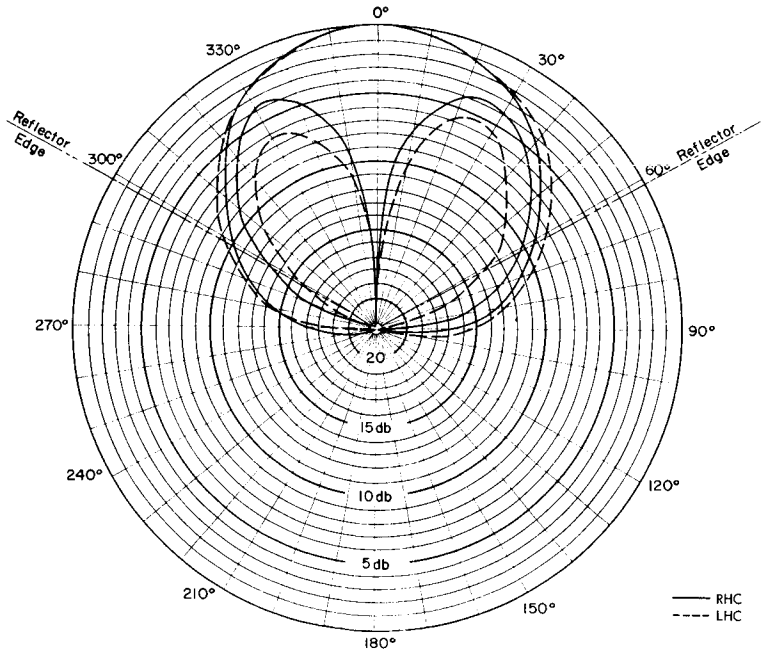

Figure 19. Primary Pattern-235 Mc

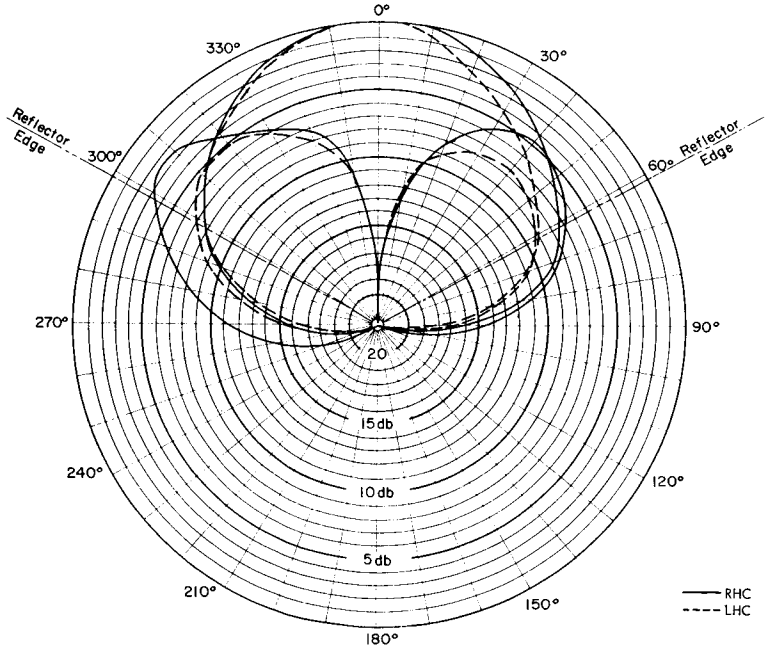

Figure 20. Primary Pattern-406 Mc

2.6-db space taper for a reflector with f/D = 0.42 has been added to the values in Table 3.

Table 3

Reflector Edge Illumination

f_o (Mc)	Sum Mode (db)		Difference Mode (db)	
	LHC	RHC	LHC	RHC
136	19.6	18.6	13.1	11.6
235	9.6	12.1	17.6	14.0
406	11.0	10.0	10.6	8.0

It can be seen that average edge illumination is 13.8 db for the sum mode and 12.6 db for the difference mode.

The primary pattern gain was measured by means of comparison to tuned half wave dipoles cut for operation at 136.5, 235, and 406 Mc. These dipoles had been previously calibrated by the identical antenna substitution method. Figure 21 shows measured gain at the operational frequencies; the average gain is

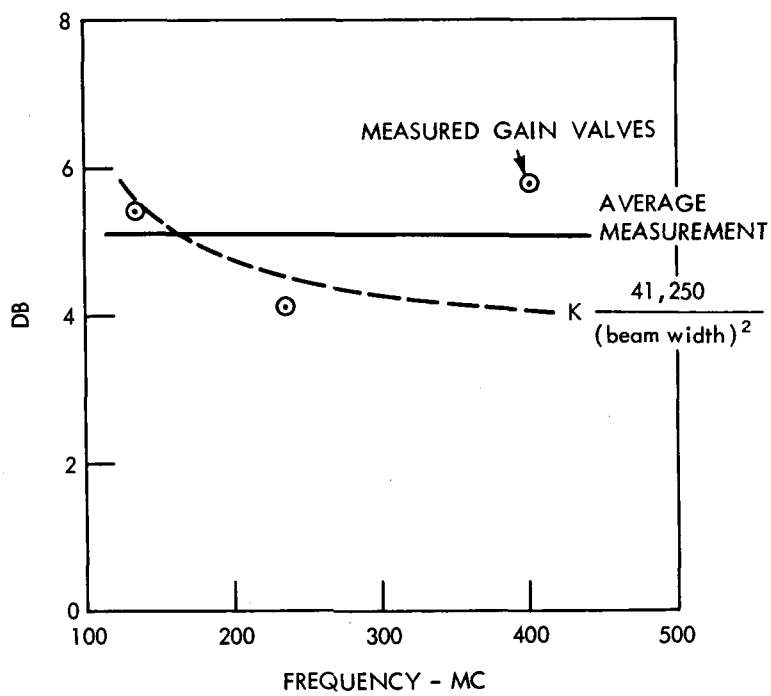

Figure 21. Primary Pattern Gain

5 db above an isotropic source. Gain and beamwidth should be constant with frequency change for the log-spiral antenna. Some variation in beamwidth can be seen in Figures 18, 19, and 20. The gain computed from these beamwidths is also plotted in Figure 21 for comparison

Primary pattern polarization ellipticity was measured by rotating tuned linear dipoles in the field of the planar log-spiral antenna. It was found that the ratio of the two linear components of field strength, in orthogonal planes, was generally less than 1 db. Table 4 lists measured polarization ellipticity.

Table 4

Primary Pattern Polarization Ellipticity

f_o (Mc)	Rotation	Ellipticity Ratio (db)
136	RHC	1.4
136	LHC	0.8
235	RHC	0.8
235	LHC	0.7
406	RHC	0.8
406	LHC	0.7

The resultant "crossed polarization" (circular polarized component of the opposite sense of rotation) for ellipticity ratios of 1.4, 0.8, and 0.7 db is 21.7, 26.0, and 28.0 db, respectively.

The coalignment of the primary difference pattern RF boresight and mechanical axis of symmetry was measured by comparison to an optically established mechanical axis. Table 5 shows the measured results and the variation of the RF boresight with changes in frequency and polarization.

Table 5

Primary Difference Pattern RF Boresight Error

f_o (Mc)	Rotation	Azimuth Error (degrees)	Elevation Error (degrees)
136	RHC	0	0
136	LHC	-1.0	+0.5
235	RHC	+0.5	0
235	LHC	0	0
406	RHC	+1.0	0
406	LHC	0	0

Inspection of Table 5 indicates that no systematic boresight errors exist and errors appear to be random. A continuous shift of azimuth boresight error with frequency change for right-hand circular polarization is the only systematic trend of error. Anticipated secondary pattern boresight error can be computed by dividing the errors in Table 5 by the compression ratio (CR) which is defined as the ratio of secondary pattern beamwidth to primary pattern beamwidth. Compression ratios and anticipated secondary pattern boresight error are listed in Table 6.

Table 6

Computed Secondary Pattern Boresight Error

f_o (Mc)	CR	Rotation	Secondary Pattern Error	
			Azimuth (mills)	Elevation (mills)
136	$\frac{50°}{6.0°} = 8.33$	RHC	0	0
		LHC	-2.1	+1.0
235	$\frac{67°}{3.96°} = 16.9$	RHC	+0.5	0
		LHC	0	0
406	$\frac{60°}{1.98°} = 30.3$	RHC	+0.6	0
		LHC	0	0

The maximum boresight error to be expected when this feed is properly installed in an 85-foot reflector can be seen to be 2.1 milliradians, or 0.12 degrees.

Secondary Patterns

Secondary patterns were measured after the feed had been installed in the TOS 85-foot reflector antenna at Wallops, Virginia, in January 1966. Figure 22 shows the feed being lifted into the reflector. The lower edge of this reflector is visible in the right background. Figure 23 is a closeup showing the feed installed at the focus of the reflector. It was not possible to focus the feed and to measure far field patterns against the collimation tower at this site because it is located only 550 feet from the 85-foot antenna; moreover, the field-generating antenna located atop the collimation tower is only 59 feet above the X-axis and common terrain. As a result, the source was in the near field at both 136 and 225 Mc and serious specular reflection from the earth distorted the pattern. As an alternative, a Bell 47G2A1 helicopter carrying a crossed log-periodic dipole structure as a field-generating source hovered above the antenna. This procedure proved suitable for measuring patterns. The helicopter could be tracked at either 136 or 235 Mc, and because two receivers and two antenna

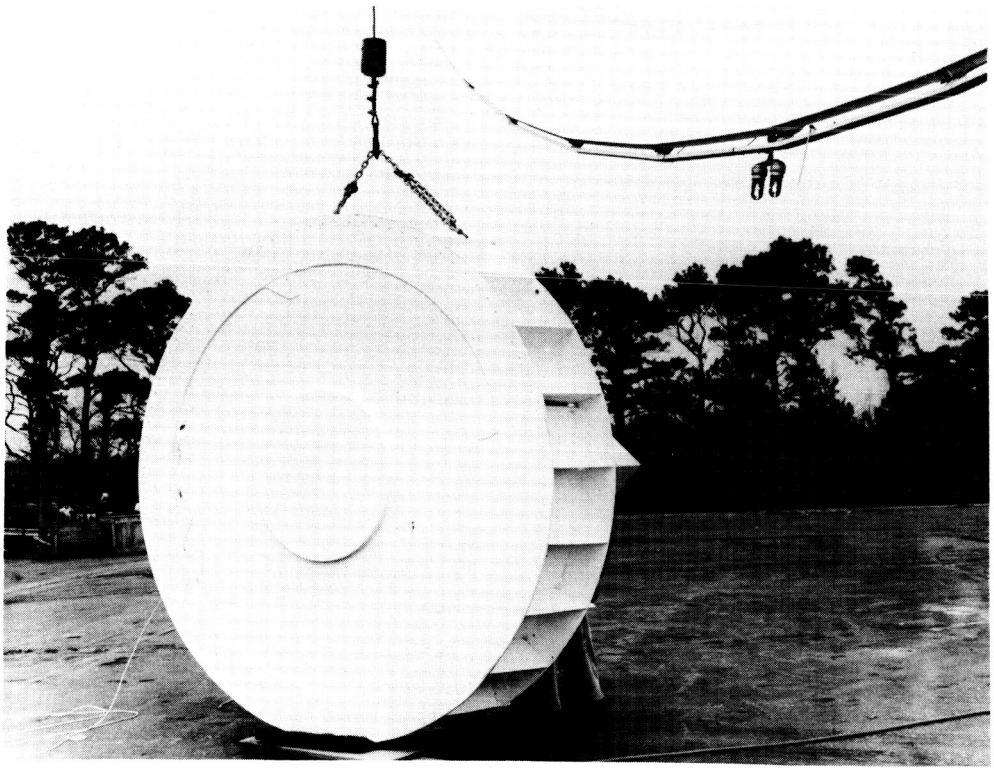

Figure 22. Feed Being Installed into Reflector

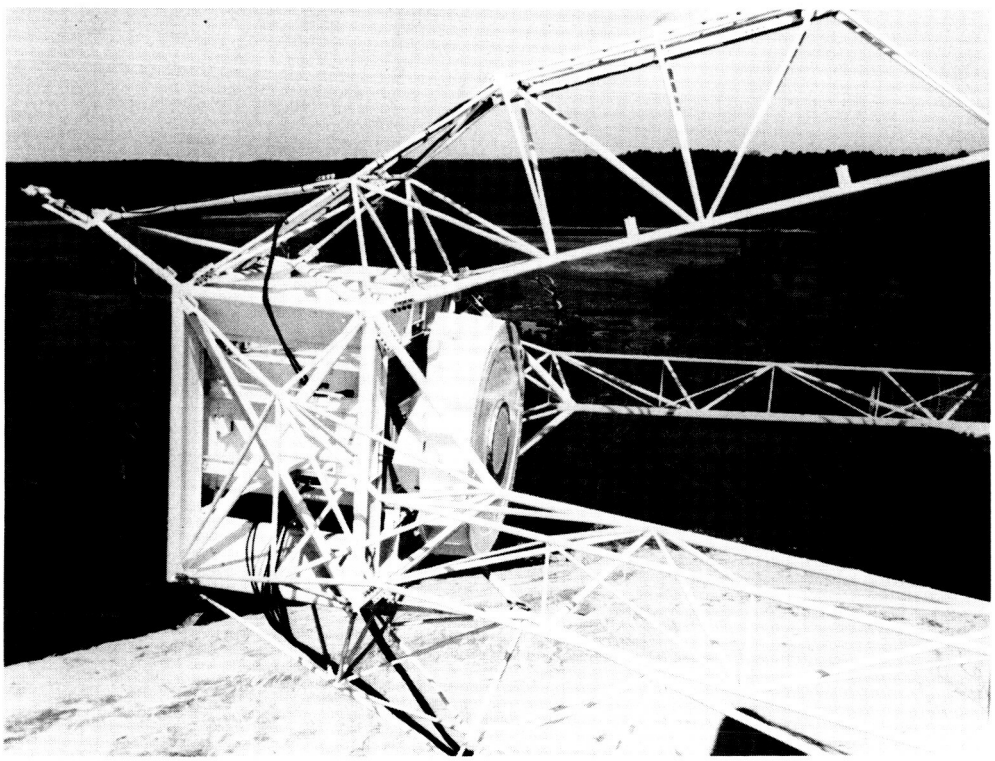

Figure 23. Closeup of Feed Installed at Focus of Reflector

pattern recorders were used, sum and difference patterns could be recorded simultaneously for any one frequency. The helicopter hovered at a range of 2000 feet for measuring patterns at 136 Mc and at 3500 feet for measuring patterns at 235 Mc. The antenna was moved about the X-axis as well as about the Y-axis. Although the helicopter was relatively stable in position, some drift due to wind occurred. Patterns were plotted from the zenith position outward and on one side only; the two "half patterns" were then combined to form the patterns shown in this report.

Figures 24, 25, and 26 are theoretical patterns obtained by solution of the Fourier integral defining the distribution at 136, 235, and 406 Mc. An aperture distribution of $b + (1-r^2)^4$ was assumed for the sum pattern, and

$$\sin\left(c\,\frac{r}{\sqrt{r^2 + .310}}\right)$$

for the difference pattern. The pedestal height b was selected to be 0.28 for an 11-db sum pattern edge taper. The quantity r is the normalized radius of the circular aperture and $c = 3.15$ is the constant establishing the difference pattern edge taper as 8 db. Sidelobes can be seen to be 34 db, 30 db, and 28.5 db, respectively, at 136, 235, and 406 Mc. The 6 db difference in level between sum and difference pattern peak intensity is characteristic of a two-channel monopulse system. The effective linear aperture blockage ratio, due to feed and support structure, is estimated to be 0.23 (10 percent due to the feed and 13 percent due to the quadrapod). The increase in sidelobe level from this blockage is computed by expression (9) to be 17 db. The new sidelobe level is approximately

$$20 \log \left[\frac{V + 2B^2}{1 - 2B^2}\right], \qquad (9)$$

where V is the sidelobe level of the unperturbed pattern and B is the aperture blockage. Sidelobe levels resulting from blocking are shown as dashed lines on the sum patterns (Figures 24 and 25).

Figures 27 through 30 are the measured patterns at 136.5 Mc for both polarization senses and about each axis. Beamwidths at 136.5 Mc were measured to be 5.4 degrees, slightly wider than the theoretical 5 degrees. Sidelobe levels of sum patterns are generally 14 db down from peak intensity. This is 3 db higher than the theoretical level determined by applying the blockage effects to the theoretical pattern (Figure 24). Difference pattern sidelobes are 14 to 18 db below the peak intensity of the difference pattern and 20 to 24 db below the peak intensity of the related sum pattern. Figures 31 through 34 present the same data for 235 Mc; the 3.3 degree beamwidth is 0.4 degrees wider than theoretical.

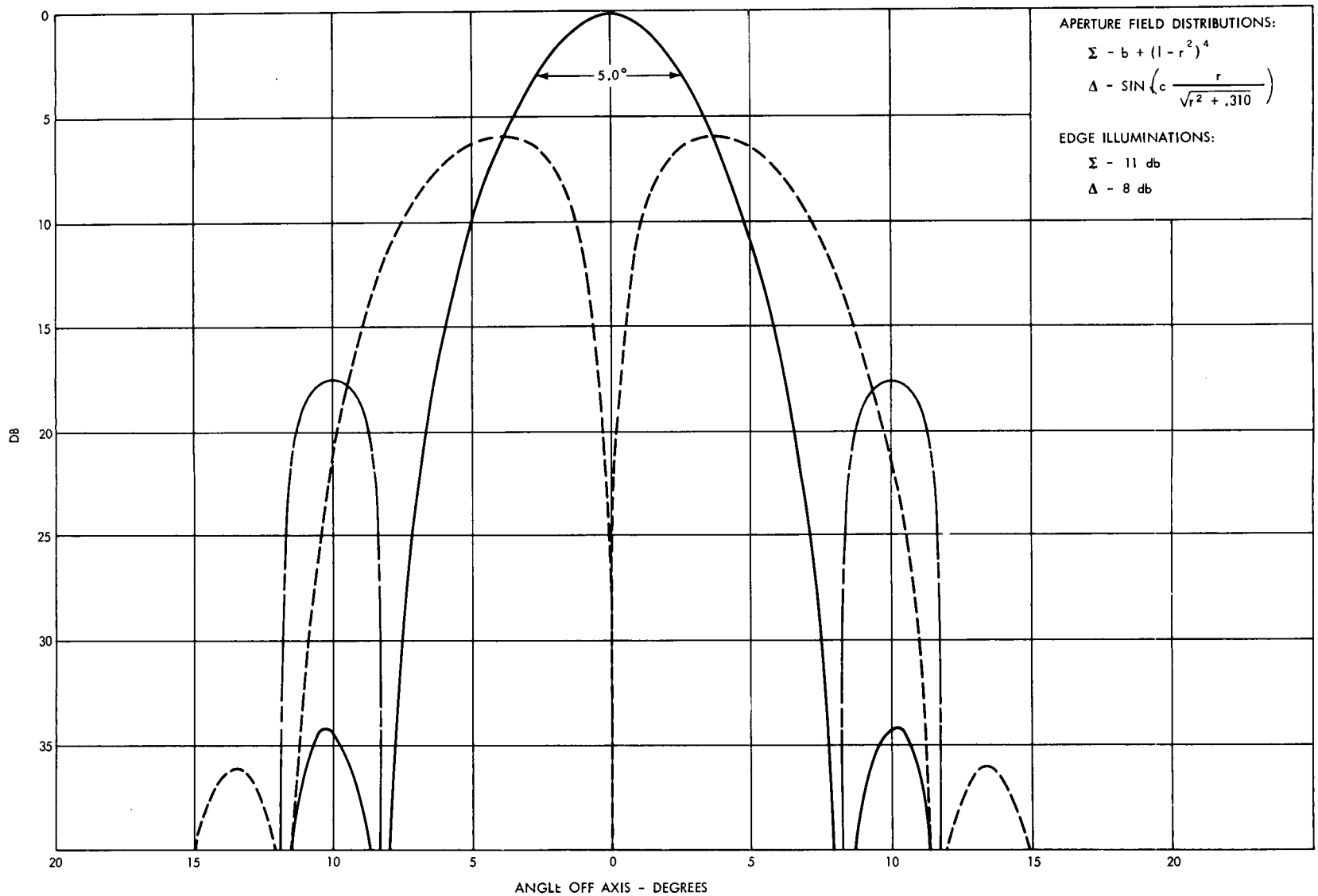

Figure 24. Theoretical Secondary Pattern-136.5 Mc

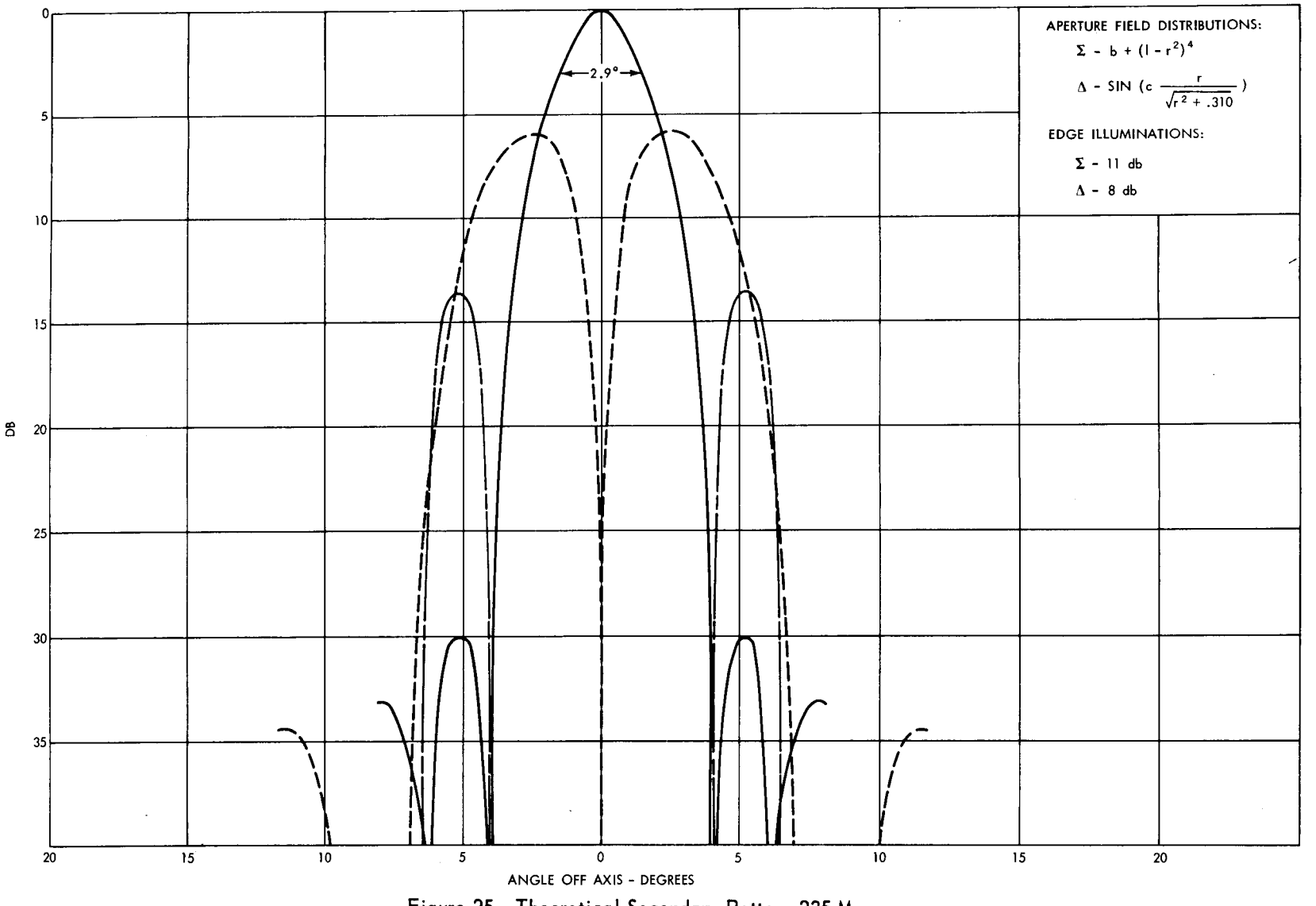

Figure 25. Theoretical Secondary Pattern-235 Mc

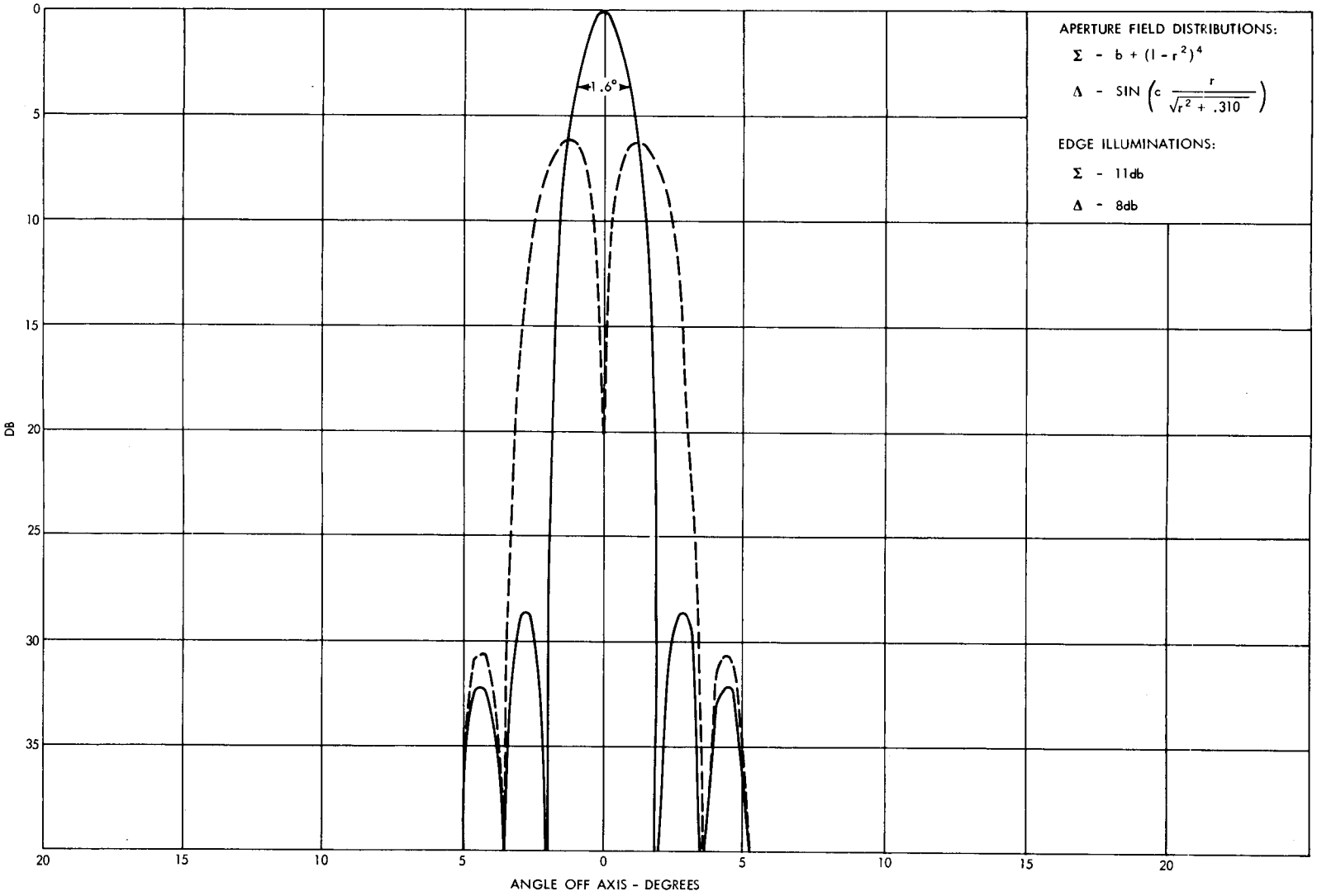

Figure 26. Theoretical Secondary Pattern-406 Mc

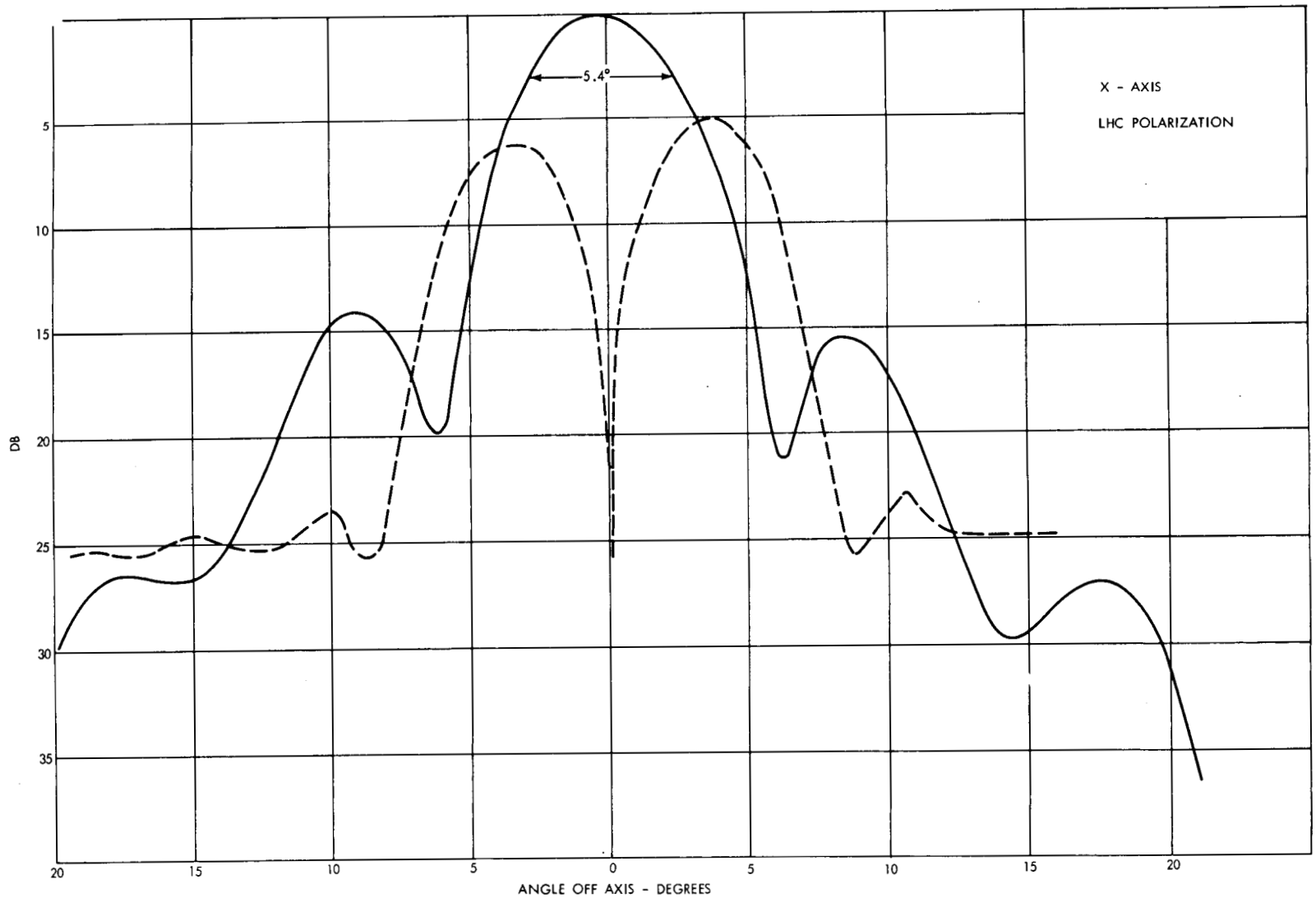

Figure 27. Measured Secondary Pattern-236.5 Mc, X-Cut, LHC Polarization

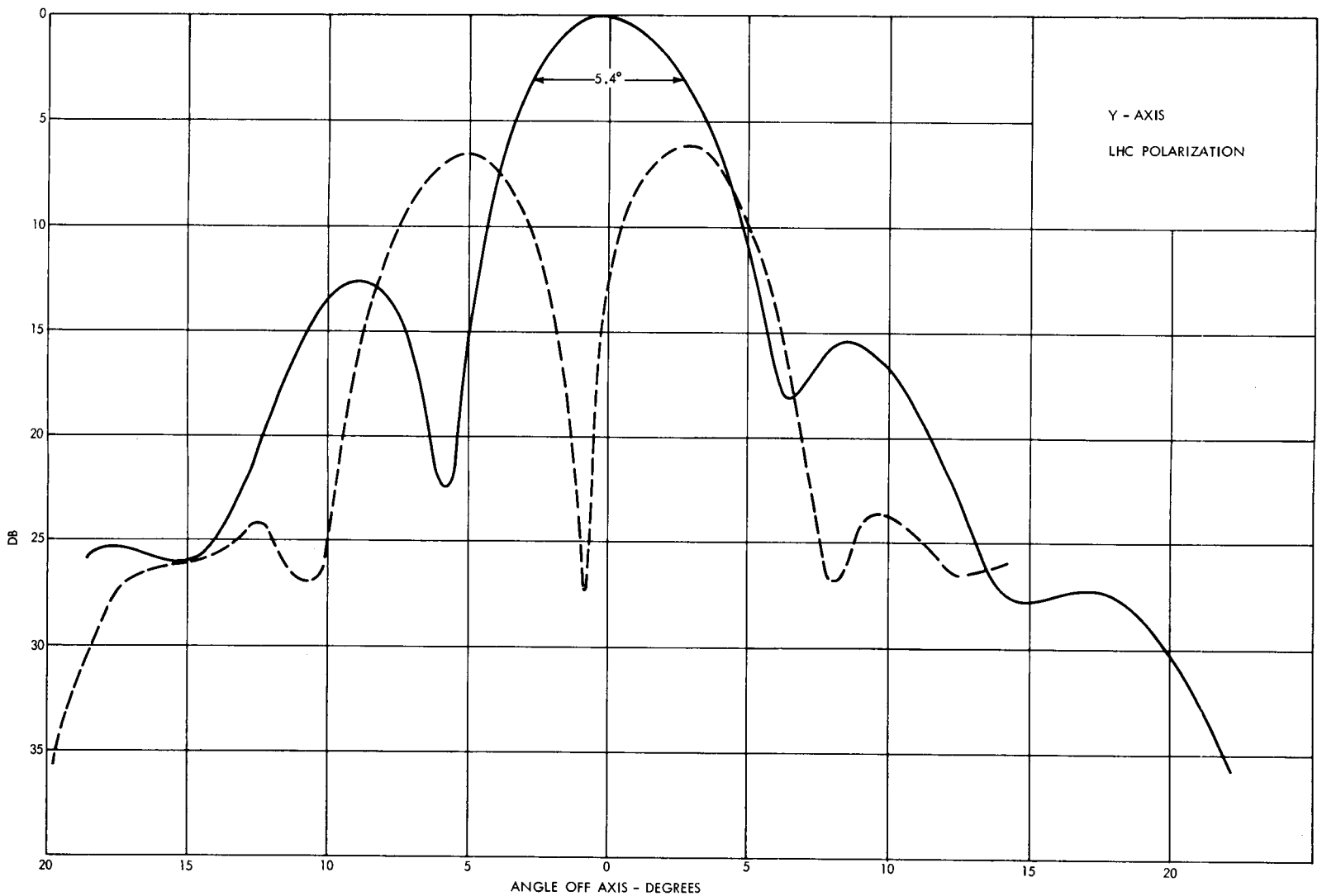

Figure 28. Measured Secondary Pattern-136.5 Mc, Y-Cut, LHC Polarization

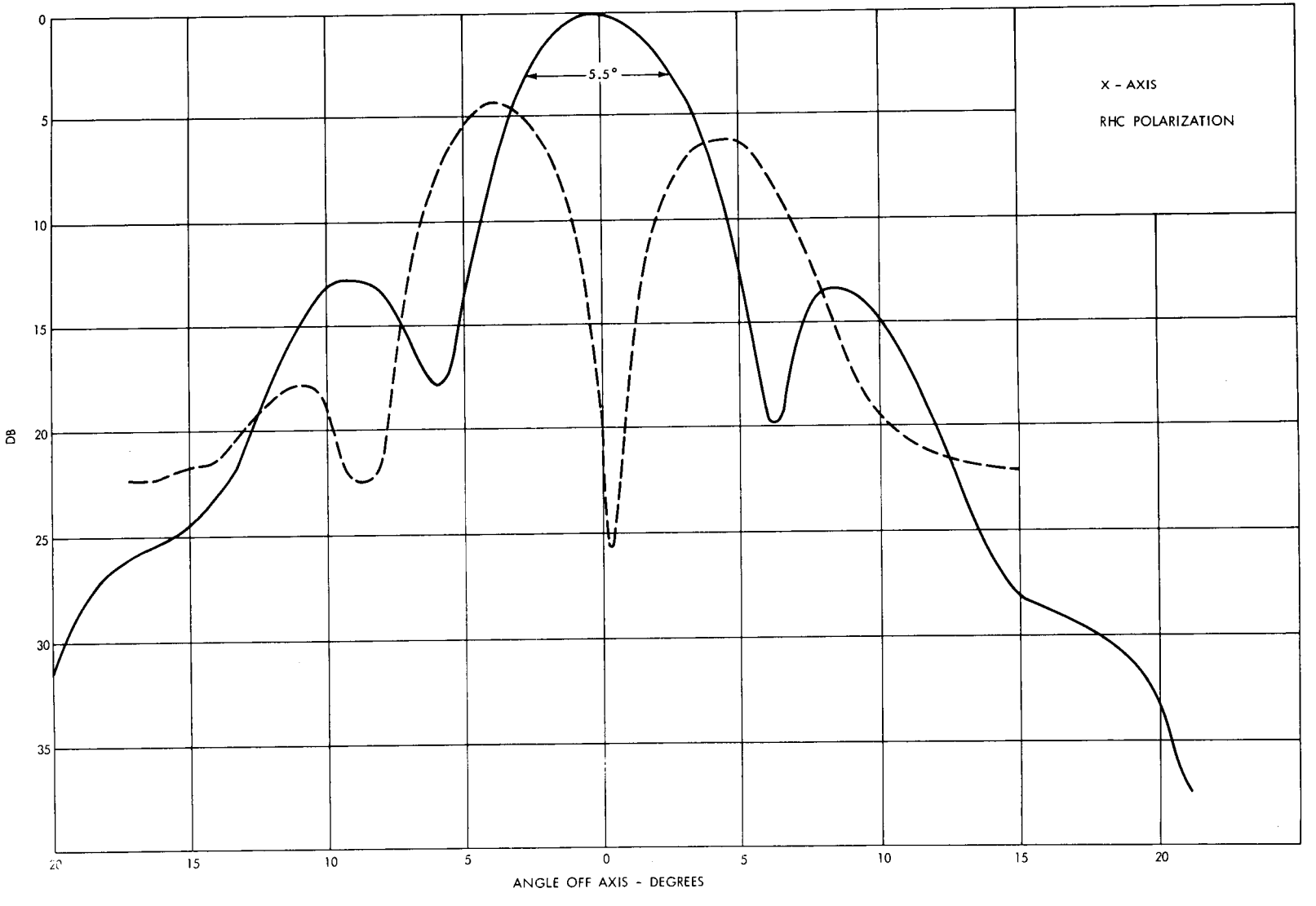

Figure 29. Measured Secondary Pattern-136.5 Mc, X-Cut, RHC Polarization

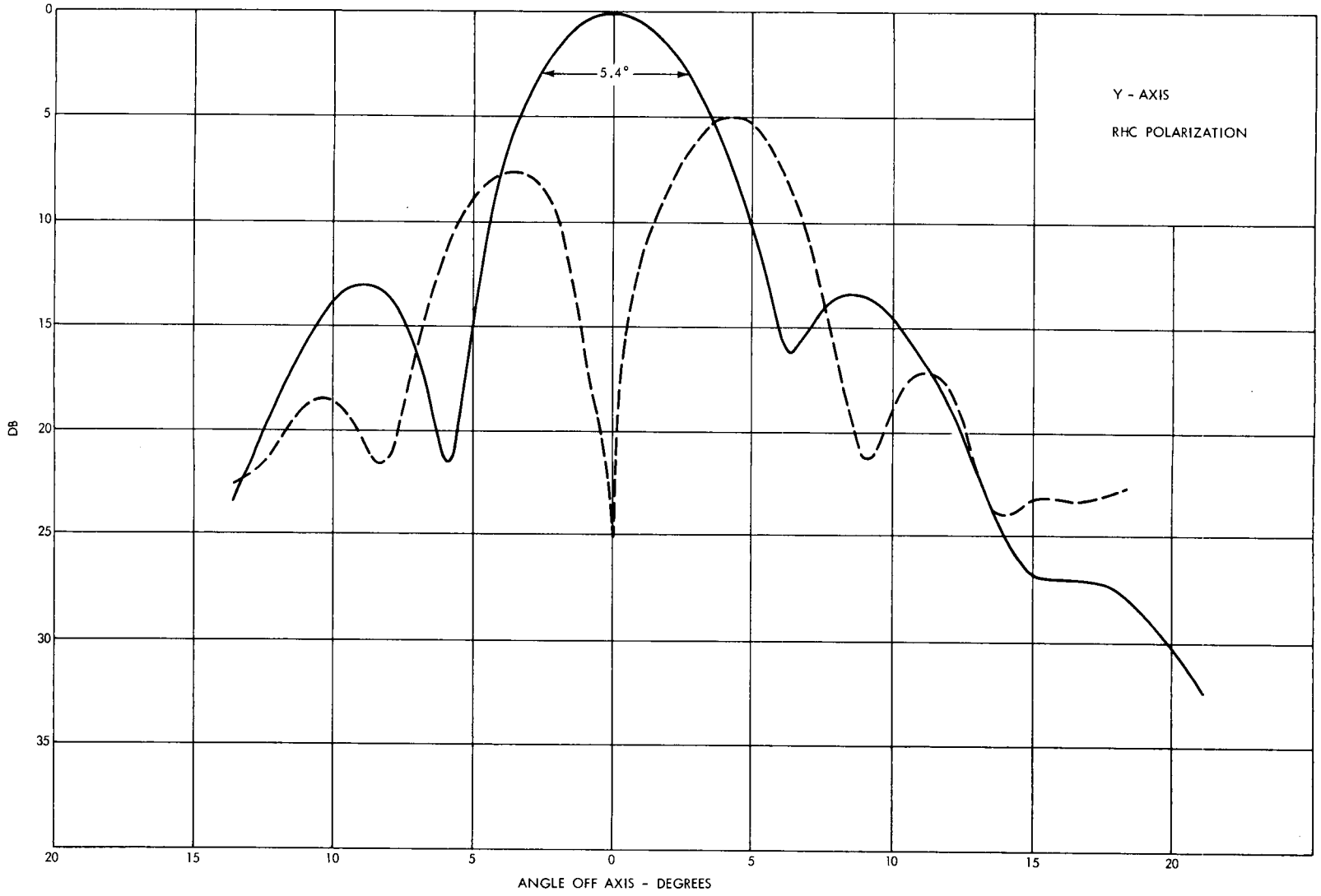

Figure 30. Measured Secondary Pattern-136.5 Mc, Y-Cut, RHC Polarization

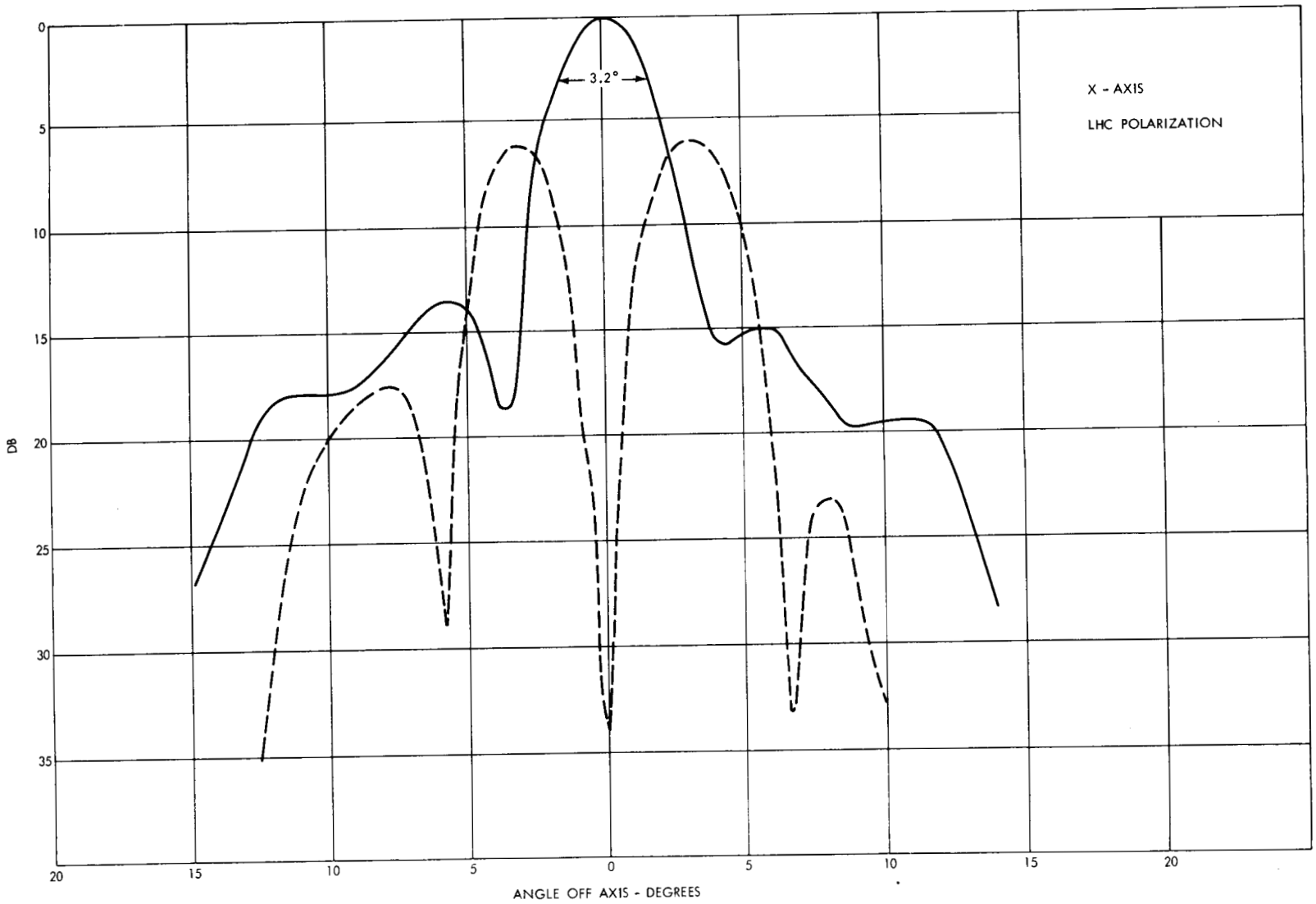

Figure 31. Measured Secondary Pattern-235 Mc, X-Cut, LHC Polarization

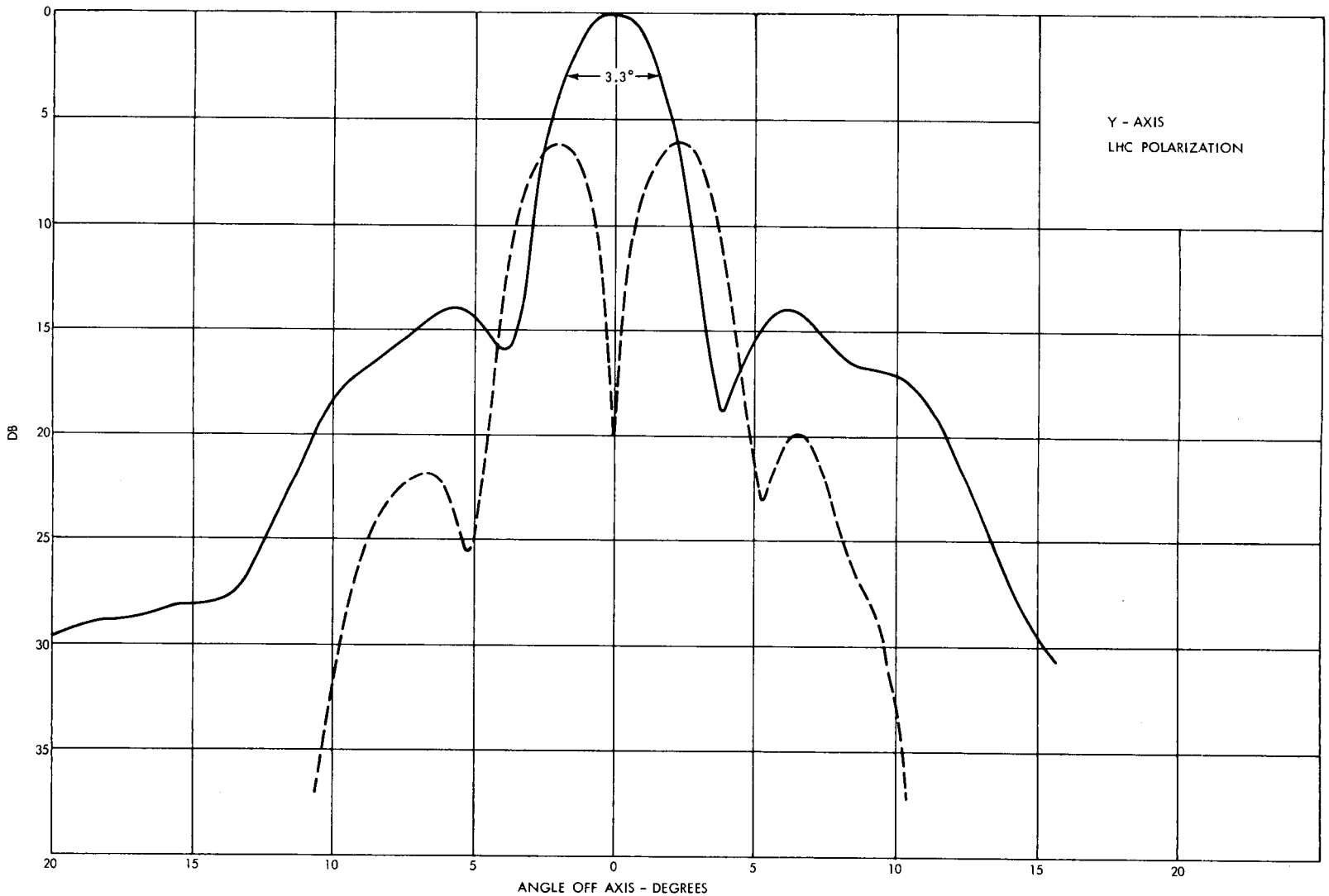

Figure 32. Measured Secondary Pattern-235 Mc, Y-Cut, LHC Polarization

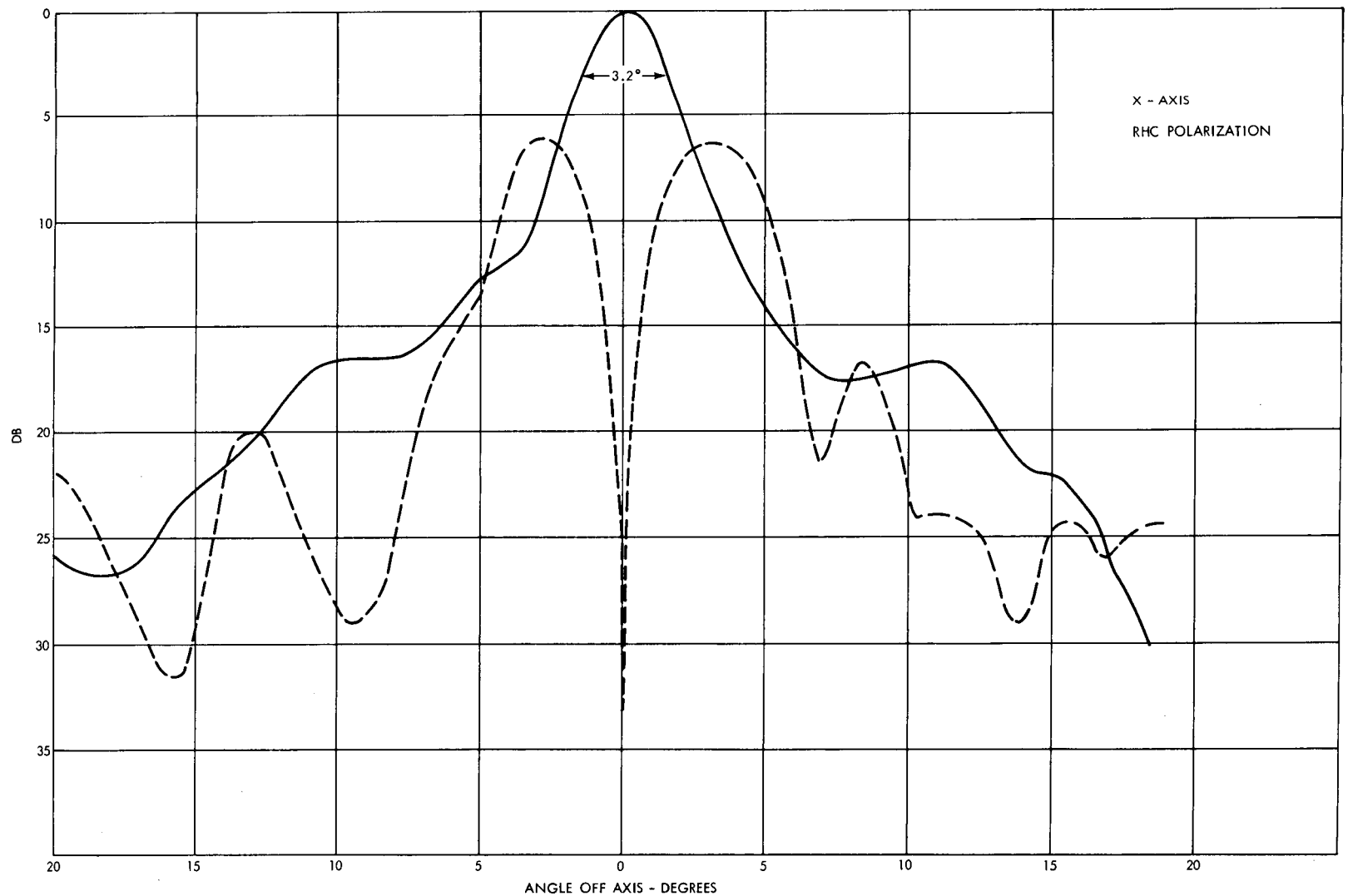

Figure 33. Measured Secondary Pattern-235 Mc, X-Cut, RHC Polarization

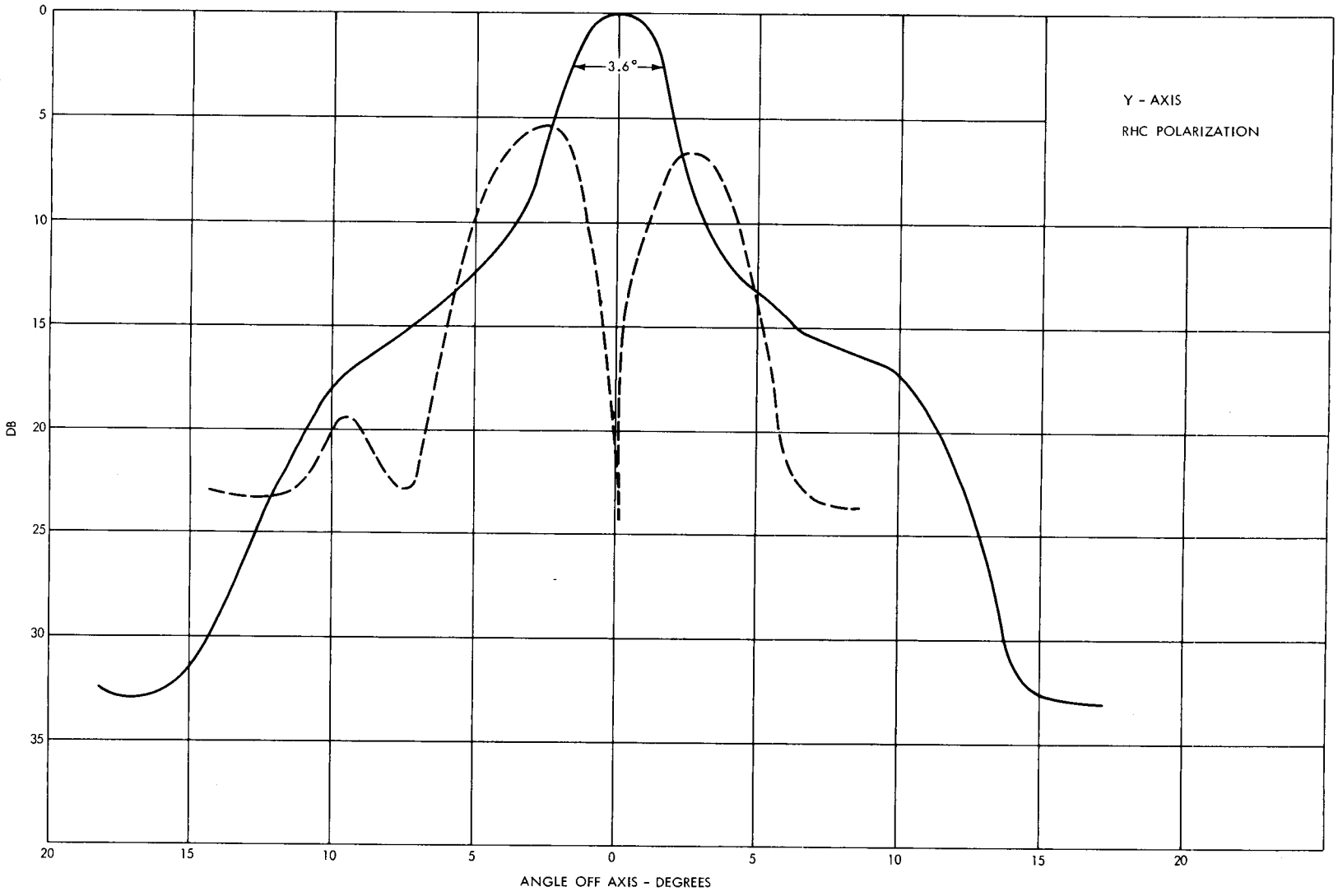

Figure 34. Measured Secondary Pattern-235 Mc, Y-Cut, RHC Polarization

Sum pattern sidelobes are also approximately 14 db down from the sum pattern peak intensity. Difference pattern sidelobes average 14 db below the peak intensity of the difference pattern and 20 db below the peak intensity of the related sum pattern. Pattern performance at 235 Mc is equivalent to that obtained with a crossed dipole feed in similar 85-foot paraboloidal reflector antennas at other locations. Performance is much better at 136 Mc than that obtained with crossed dipole feeds, when sidelobes have been as high as 7 db.

Gain and Efficiency

The gain of the reflector with the feed installed was not measured; however, telemetry recordings from TIROS IX indicated a 2-db improvement over data received with the crossed dipole fed reflector at Fairbanks, Alaska. The gain of the antenna at Alaska has been measured to be 26 and 30 db at 136 and 235 Mc, respectively. If the gain of the reflector fed with the log spiral is indeed 28 and 32 db, the efficiency is 46 percent and 49 percent at 136 and 235 Mc, respectively.

Impedance Characteristics

The impedance characteristics of the feed were not measured with the feed installed in the reflector but with the feed radiating into free space. Figure 17 shows the feed and complete RF system arranged for this purpose. Figures 35 and 36 present impedance data for the sum and difference channels and are referred to the diplexer output terminal (receiver side) for each measured point. Data are plotted on expanded Smith charts to show the detail of the well-matched condition; however, this resulted in two points falling off the chart for difference channel data (Figure 36). The impedance components are 0.4 - j.34 ohms for right-circular polarization at 136 Mc and 0.58 + j.55 ohms for left-circular polarization at 235 Mc. Voltage standing-wave ratios were checked with the feed installed in the reflector and these compared favorably with the data plotted in Figures 35 and 36.

Wave Polarization

In general, the energy received (or transmitted) by any antenna is elliptically polarized and true circular (or linear) polarization is not possible over a broad band of frequencies. The elliptically polarized wave on axis in the far field is considered to be composed of two orthogonal linear components. The terminal point of the field vector, rotating in space, describes the polarization ellipse; the voltage axial ratio of the polarization ellipse is the ratio of the major and minor axes of this ellipse. It was considered that the secondary pattern axial ratio of this antenna should not exceed 2 db over the specified 4:1 band of frequencies.

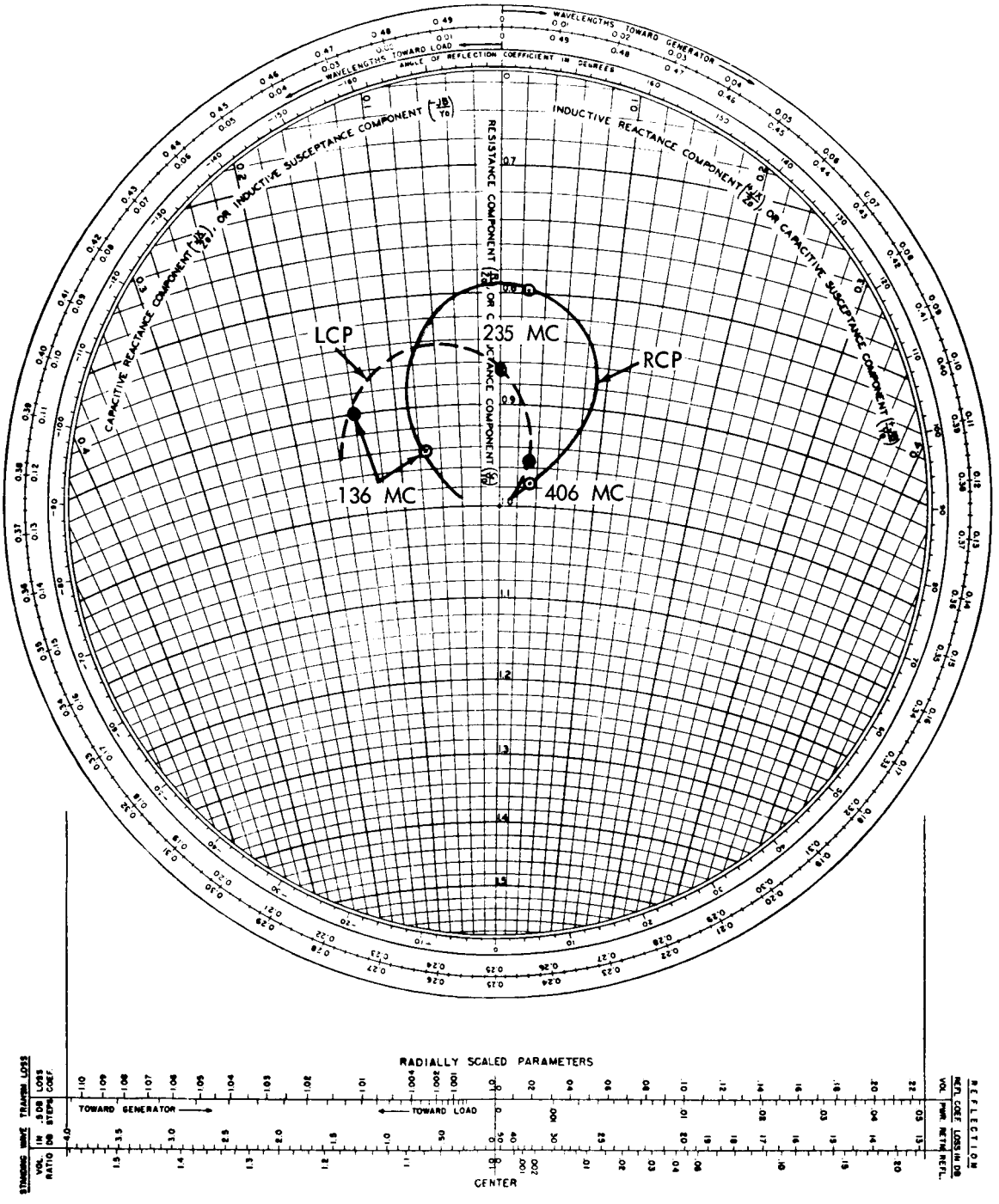

Figure 35. Sum Channel Input Impedance

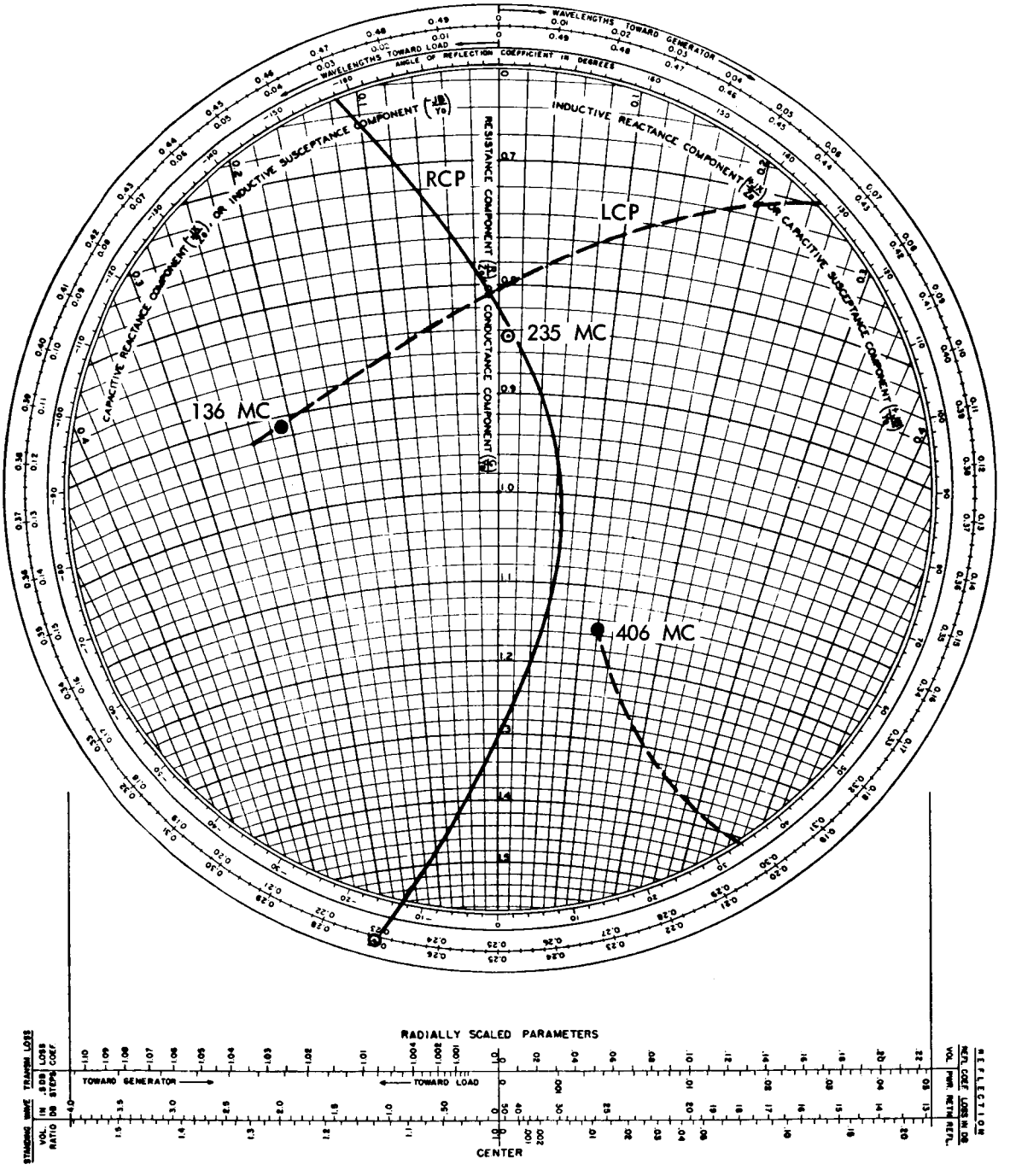

Figure 36. Difference Channel Input Impedance

Techniques for determining the polarization axial ratio do not provide precise measurement. Errors are introduced by spurious reflection from the range as well as by propagation anomalies. A linear dipole, rotating at 0.5 rpm, was provided atop the collimation tower at Wallops, Virginia, for measuring polarization axial ratio. It was observed that the axial ratio was somewhat higher than the anticipated 2.0 db. Because the antenna main beam "sees" the earth in front of it, it is reasonable to assume that the effect observed was at least in part due to a change in specular reflection from the ground as the dipole was rotated. Moreover, the rate of rotation was so slow that some receiver drift occurred during one revolution. Table 7 lists the measured axial ratios.

Table 7

Axial Ratio of Sum Pattern Polarization Ellipse

f_o (Mc)	Rotation	Axial Ratio (db)
136	LHC	2.1
136	RHC	3.3
235	LHC	2.4
235	RHC	7.8

The gross disparity at 235 Mc for the right-hand sense of rotation is not explainable, particularly in view of the excellent impedance characteristics shown in Figure 35 for this output terminal. Deterioration of a contact terminal point is suspected; however, time did not permit an analytic investigation.

Boresight Characteristics

A common problem with two-channel monopulse systems is instability of the difference pattern null position. If it is assumed that no structural errors exist, then misalignment of the RF and optical boresight can be attributed only to precomparitor phase errors or coupling errors. A thorough analysis by Charitat (ref. 22) demonstrates that the significant cause of RF boresight shift is coupling, and that RF boresight shift due to precomparator phase error is insignificant.

Gross RF boresight shift results from the coupling errors caused when spurious reflections from the range enter a monopulse feed. This condition is discussed by Thompson (ref. 23) who shows that RF boresight shift can be as much as 4.5 milliradians when the spurious reflection is 15 db down from the direct signal, and 8.0 milliradians when it is 10 db down. RF boresight errors

of this magnitude were observed when the feed was installed in the reflector at Wallops, Virginia. Figure 37 is a plot showing the deviations of RF boresight from optical boresight for the two frequencies and the two senses of polarization involved. The maximum deviation of the RF boresight from the optical axis can be seen to be 11.9 milliradians. Analysis of primary pattern boresight error (Table 5) predicted a maximum secondary pattern boresight error of 2.1 milliradians. The excessive error of 9.8 milliradians would be indicative of spurious reflection greater than 10 db from the range when Thompson's (ref. 24) analysis is applied. Although the maximum tolerable misalignment of RF and optical boresight had not been specified, the shift of RF boresight with frequency change was specified and is compared with measured boresight shift in Table 8 which lists the shift of RF boresight in changing from 136 to 235 Mc.

Table 8

Measured Shift of RF Boresight with Frequency Change

Antenna Mount Axis	Rotation Sense	Boresight Shift (mills)	Specification (mills)
X	LHC	± 2.3	± 3.5
X	RHC	2.1	3.5
Y	LHC	0.9	3.5
Y	RHC	11.7	3.5

The error about the Y-axis for right-circular polarization can be seen to be excessive. The shift of RF boresight with polarization change was measured at 136 Mc as well as at 235 Mc about each axis of the antenna mount. It was specified that this shift should not exceed 3 percent of the related sum pattern half-power beamwidth. Table 9 presents the measured data for change from right-circular to left-circular polarization.

Table 9

Measured Shift of RF Boresight with Polarization Change

f_o (Mc)	Antenna Mount Axis	Measured Shift (mills)	Specified Maximum Shift (mills)
136	X	14.0	2.8
136	Y	11.0	2.8
235	X	5.2	1.6
235	Y	10.5	1.6

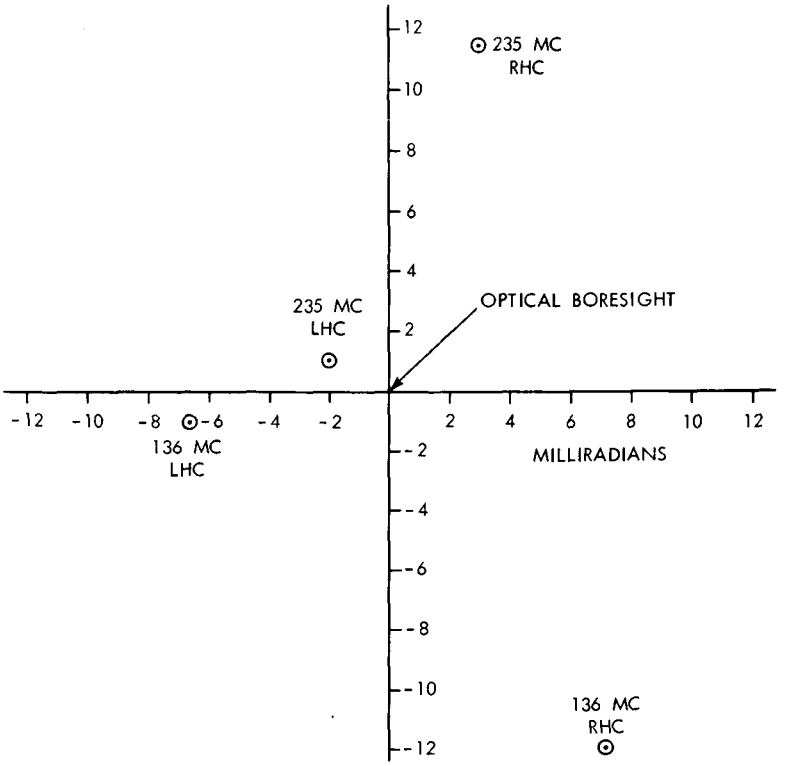

Figure 37. Comparison of RF and Optical Boresight Axes

The observed shift of RF boresight with polarization change can be seen to be excessive.

Tracking Tests

To demonstrate tracking capability of the primary feed and RF system, this equipment was mounted on an Antlab 3004-CT elevation-over-azimuth pedestal located on the roof of the contractor facility at Alexandria, Virginia. A modified Teledyne 105A tracking receiver completed the two-channel monopulse system. The Goddard calibration aircraft DC-4 No. 27, carrying a 136-Mc beacon, was flown over the antenna on two consecutive days, October 28 and 29, 1965. Figure 38 shows portions of the tracking record and indicates variations of ±1.5 degrees in azimuth and elevation. Tracking was accomplished at various ranges of the aircraft from one-half mile to five miles, and at angular speeds of three degrees per second to one degree per second. The feed readily acquired the target and did not lose track during the operation. Findings were somewhat inconclusive because of serious multipath reflections from the roof of the building on which the feed was mounted.

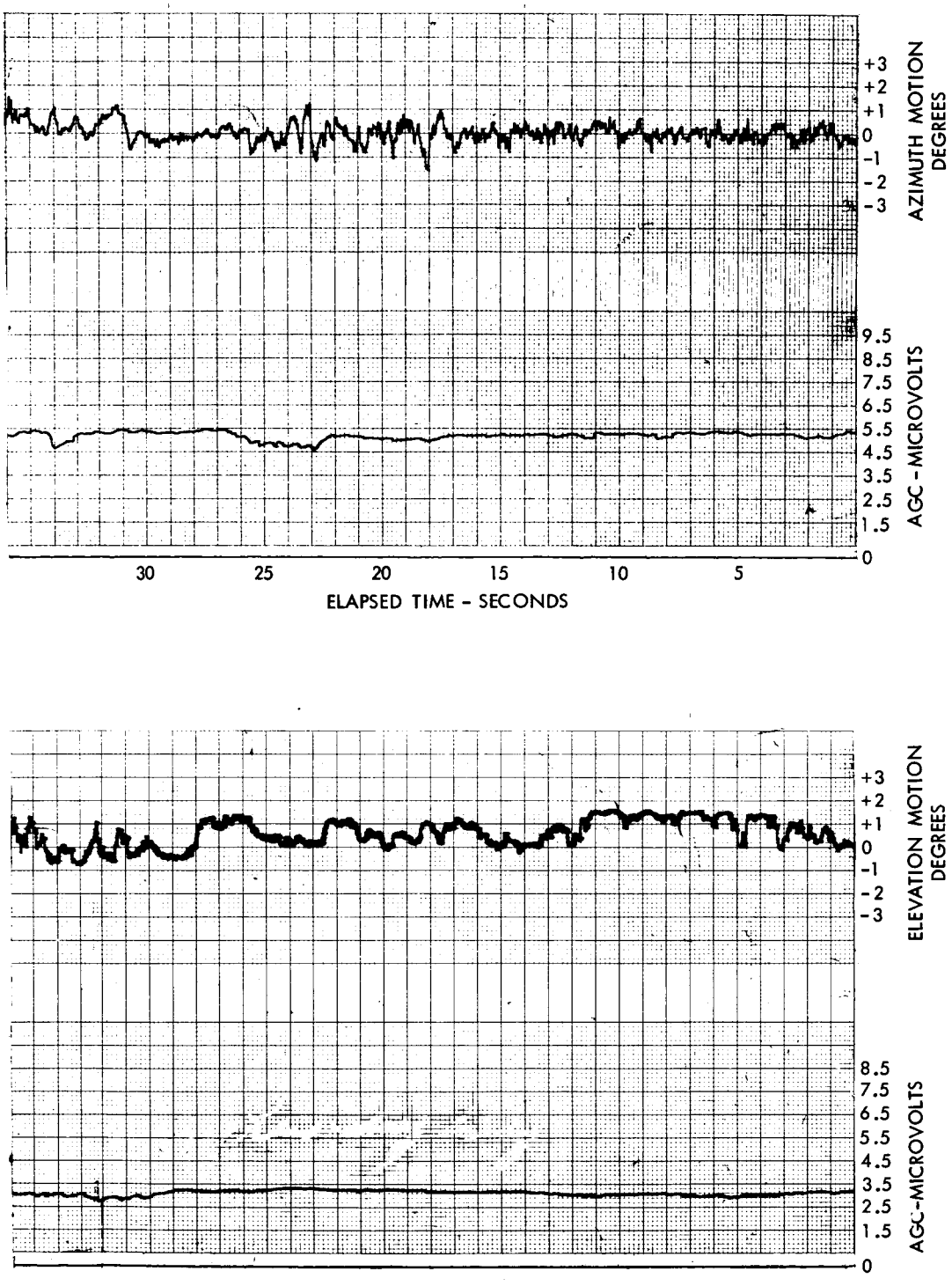

Figure 38. Primary Feed Tracking Records-136.5 Mc

Additional tracking tests were conducted in April 1966, after the feed had been installed in the reflector at Wallops, Virginia. The RF system and receivers shown in Figure 9 were used for these tests and the calibration aircraft was operated at 10,000 feet altitude. The antenna system tracked the aircraft reasonably well at 136 Mc using either the ITTFL 4003 receiver or the General Dynamics SC-762 receiver as the tracking receiver. Moreover, a reversal of the polarization of the RF wave received at the antenna, from right circular to left circular polarization, gave properly phased tracking system servo error voltages with the proper polarity. An RF boresight shift of approximately 0.7 degrees was observed, however, in changing the sense of polarization. In addition, pointing fluctuations about the X, as well as the Y axis, of approximately 0.5 degrees RMS were observed in tracking TIROS IX (orbit number 5295) on April 5, 1966. Tracking the aircraft at 235 Mc was not satisfactory using either receiver, and the reason for this failure is not understood. It is believed the difficulty was in the feed. One satisfactory track of TIROX IX (orbit number 5307) was accomplished at 235 Mc on April 6, 1966, ruling out any basic design anomaly.

As a result of apparent RF boresight error, excessive polarization axial ratio, and inability to track at 235 Mc, the feed was not retained in the Wallops, Virginia, reflector for use with TIROS Operational Satellites.

FUTURE PLANS

It is planned to continue developmental effort on the cavity-backed log-spiral feed for reflector antennas. This effort will be directed toward improvement of axial ratio and RF boresight characteristics and increase in operation bandwidth. A feed operating over the frequency band 136 to 2300 Mc is envisioned.

CONCLUSIONS

It is concluded that a planar log-spiral feed is a superior feed for reflector antennas having a circular aperture. The feed pattern, being circularly symmetric, provides equal edge illumination around the entire aperture. Sum and difference pattern edge illumination can be made nearly equal and can easily be adjusted for any desired value. Reduction in antenna temperature and increased antenna efficiency result. Both senses of circular polarization can be received simultaneously with no 3-db loss and without RF transmission line switches. Additional developmental work is required to perfect the design. This can readily be done by means of scale models of feeds in reflectors.

ACKNOWLEDGMENT

The author acknowledges the contribution of Julius A. Kaiser to this report.

REFERENCES

1. Dyson, J. D.: The Equiangular Spiral Antenna. Technical Report 21, Antenna Laboratory, University of Illinois, September 15, 1957.

2. Dyson, J. D.: Recent Developments in Spiral Antennas. Proceedings of National Aeronautical Electronics Conference, Dayton, Ohio, May 4, 1959.

3. Dyson, J. D.: Multi-Mode Logarithmic Spiral Antennas. Proceedings of National Electronics Conference, Chicago, Illinois, October 10, 1961, pp 206-213.

4. Radiation Systems, Inc.: Final Report to Contract NAS5-9788. Technical Report TR-82, February 11, 1966.

5. Turner, E. M.: Spiral Slot Antenna. U. S. Patent No. 2863145, December 2, 1958.

6. Rumsey, V. H.: Frequency Independent Antennas. IRE National Convention Record, Part 1, 1957, pp 114-118.

7. Du Hamel, R. H.; and Isbel, D. E.: Broadband Logarithmically Periodic Antenna Structures. IRE National Convention Record, Part 1, 1957, pp 119-128.

8. Dyson, J. D.: 1961, op. cit.

9. Shelton, J. P. Jr.; et al.: Two Channel Monopulse Antenna Feed. Final Report to Contract NAS5-1589, Radiation Systems, Inc., Technical Report TR-16-U, March 21, 1962.

10. Du Hamel, R. H.: 1957, op. cit.

11. Kaiser, J. A.: The Archimedian Two Wire Spiral Antenna. IEEE Transactions on Antennas and Propogation, Vol. AP-8, No. 3, May 1960, p 312.

12. Ranson, P. L.: An Experimental Investigation of the Four Arm Planar Logarithmic Spiral Antenna. Technical Report 65-5, Antenna Laboratory, University of Illinois, May 1965.

13. IEEE Standard No. 149, January 1965, p 6.

14. Edward, C. E. H.; and Lantz, P. A.: Noise Temperature Measurement of 40-foot and 85-foot STADAN Reflector Antennas. GSFC Report X-525-65-31, February 1965.

15. Hansen, R. C.: Low Noise Antennas. Microwave Journal, Vol. 2, No. 6, June 1959, p 19.

16. Allen, C. C.: Antenna Noise Temperature Study by Computer. General Electric Company, Final Report Contract NAS5-3909, March 2, 1965.

17. Sciambi, A. F.: The Effect of Aperture Illumination on the Circular Aperture Pattern Characteristics. Microwave Journal, Vol. 8, No. 8, August 1965, p 79.

18. Radiation Systems, Inc.: System Study of an Advanced Monopulse Antenna. Final Report to Contract NAS5-9713, December 4, 1964.

19. Cheo, B. R.; Rumsey, V. H.; and Welch, W. J.: A Solution to the Frequency Independent Antenna Problem. IRE Transactions, AP-9, November 1961, pp 527-534.

20. Dyson, J. D.; and Griswold, R. E.: Measurement of the Phase Centers of Antennas. Antenna Laboratory, University of Illinois, Report 66, Contract AF 33(657)-10474, December 1963.

21. Wheeler, Myron S.: Phase Characteristics of Spiral Antennas. IEEE Convention Record, Part II, 1964, pp 143-152.

22. Charitat, Jene Jr.: A Comparison of Monopulse and Conical Scanning Tracking Systems. Radiation Systems, Inc., Technical Report TR-84, April 1, 1966, p A-7.

23. Thompson, Anthony S.: Boresight Shift in Phase Sensing Monopulse Antennas Due to Reflected Signals. Microwave Journal, Vol. 9, No. 5., May 1966, p 47.

24. Thompson: 1966, *op. cit.*

APPENDIX

PERFORMANCE CAPABILITY LIMITATIONS OF CROSSED DIPOLE FED REFLECTORS

EDGE ILLUMINATION

When crossed dipole elements (four) are used in a monopulse arrangement, optimum illumination of the reflector edges cannot be achieved for the difference pattern because the difference primary pattern lobes are generated by pairs of dipoles laterally displaced on each side of the axis of reflector symmetry. The effective aperture (two dipoles) is one-half the size of that for all four dipoles which generates the primary sum pattern; hence, the beamwidth of each primary difference lobe is twice as wide as the primary sum lobe. Moreover, the primary difference lobe is displaced off axis an amount equal to the dipole spacing, which is adjusted for best sum pattern illumination of the reflector. Consequently, if sum pattern reflector edge illumination is set to be the optimum 11.5 db, difference pattern reflector edge illumination is nearly unity. As a result, the secondary difference pattern suffers a loss in gain and an increase in sidelobe level, and degradation of the noise figure for the tracking system occurs because radiation from the warm earth (290°K) is seen by the primary difference feed.

The primary sum pattern of a four-dipole monopulse feed is not circularly symmetric because the E- and H-plane beamwidths are not equal. For the same reason, the primary difference pattern of a collinear pair of dipoles (as used to generate one monopulse primary difference lobe) is not circularly symmetric. The ellipticity of a primary difference pattern lobe can be seen to be 7 db (Figure A-1), a plot of measured E- and H-plane difference patterns of a four-dipole monopulse feed with dipoles located $\lambda/4$ above a reflecting screen. Figure A-2 presents the same data for a broadside array of four dipoles and shows ellipticity at the reflector edge to be 7-8 db. If the illumination of a reflector having a circular aperture lacks circular symmetry, spillover results causing a loss in gain, an increase in sidelobe level, and an increase in antenna temperature.

ANTENNA APERTURE EFFICIENCY

The theoretical maximum efficiency of a circular aperture fed with a four-dipole monopulse feed can be approximated to be 39 percent. This compares with measured values of efficiency of existing NASA Space Tracking and Data

Acquisition Network (STADAN) 85-foot paraboloidal reflector antennas illuminated with four-dipole feeds. Table A-1 summarizes measured results:

Table A-1

Measured Efficiencies of STADAN 85-Foot Reflector Antennas Illuminated with Four-Dipole Feeds

Frequency (Mc)	Measured Gain	Gain for k = 100 %	Efficiency - k (percent)
1705	48.0 db; 6.30×10^4	2.16×10^5	29.2
403	36.4 db; 4.36×10^3	1.22×10^4	35.8
136	26.0 db; 3.80×10^2	1.37×10^3	27.8

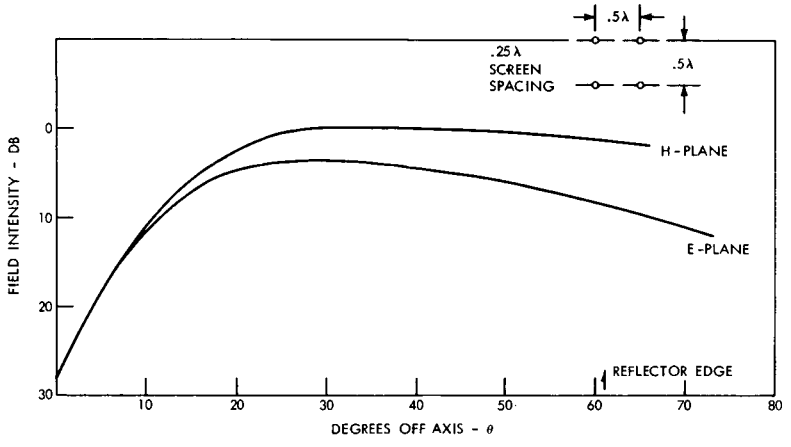

Figure A-1. Primary Difference Pattern Illumination, Four-Dipole Monopulse Feed

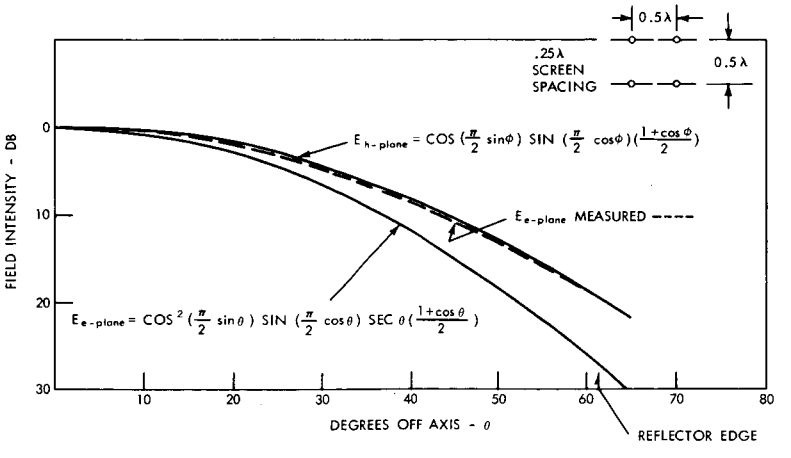

Figure A-2. Primary Sum Pattern Illumination, Four-Dipole Monopulse Feed

The primary pattern field strength for a four-dipole feed spaced $\lambda/2$ and located $\lambda/4$ above a reflective screen is given by

$$E_e = \cos^2\left(\frac{\pi}{2}\sin\theta\right)\ \sin\left(\frac{\pi}{2}\cos\theta\right)\ \sec\theta\ \left(\frac{1+\cos\theta}{2}\right), \qquad \text{(A-1)}$$

$$E_h = \cos\left(\frac{\pi}{2}\sin\phi\right)\ \sin\left(\frac{\pi}{2}\cos\phi\right)\ \left(\frac{1+\cos\phi}{2}\right), \qquad \text{(A-2)}$$

These curves are plotted in Figure A-3 and are compared with the aperture distributions $(1-r^2)^2$ and $(1-r^2)^3$, where r is normalized aperture radius. Silver* provides gain factors for these distribution and lists them to be 0.56 for the quadrature distribution and 0.44 for the cubic distribution. It can be seen that the H-plane primary pattern closely approximates the quadratic expression, especially

*S. Silver, Microwave Antenna Theory and Practice, McGraw-Hill, 1949, p 95.

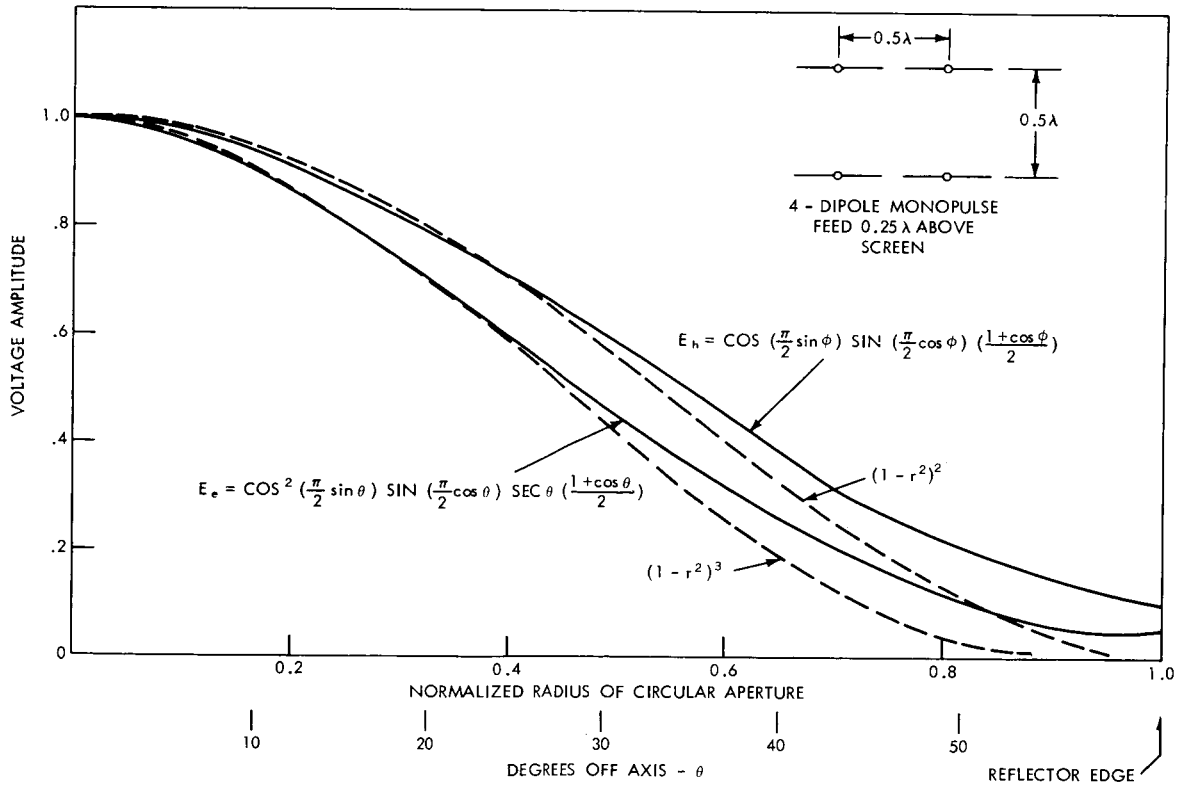

Figure A-3. Comparison of Primary Patterns and Classic Aperture Distributions

at the center of the reflector where energy is highest. Hence, the H-plane gain factor can be assumed to be 0.44. The E-plane primary pattern lies somewhat above the cubic curve; hence, the gain factor is estimated to be 0.60. The average total gain factor is then 0.55. Because the reflecting screen spillover efficiency is 0.7, the maximum aperture efficiency of the antenna is 0.7×0.55 or 39 percent.

TRACKING ERROR

Tracking error is defined to be the angular error between a straight line to a target (boresight) and the electrical axis (pattern null) of a monopulse antenna. For distinction, pointing error is defined to be the angular error between a straight line to a target and an inertial reference (such as true north), as measured by the mount. Pointing error includes tracking error. Tracking error is largely microwave error but it may include some automatic control error and some axis transformation error. The NASA calibration aircraft measures tracking error of monopulse antenna systems routinely. Typical errors (verbal discussion with John Berbert, GSFC) are listed in Table A-2.

Table A-2

Measured Tracking Error–STADAN 85-Foot Reflector Antennas

Freq. (Mc)	Measured Tracking Error	
	Degrees	Milliradians
136	± 0.33	± 5.76
400	± 0.25	± 4.36
1700	± 0.10	± 1.74
4000	± 0.07	± 1.30 (for Y-axis)
4000	± 0.03	± 0.50 (for X-axis)

These tracking errors cannot be reduced to zero with a four-dipole feed because of inability to install the dipole structure with perfect spacing off axis, as well as inability to cut precisely and maintain the RF feed lines to these dipoles.